



# Monitoring cropland daily carbon dioxide exchange at field scales with Sentinel-2 satellite imagery

Pia Gottschalk<sup>1</sup>, Aram Kalhori<sup>1</sup>, Zhan Li<sup>1,a</sup>, Christian Wille<sup>1</sup>, and Torsten Sachs<sup>1,2</sup>

<sup>1</sup>Remote Sensing and Geoinformatics, Geodesy, GFZ German Research Centre for Geosciences, 14473 Potsdam, Germany

<sup>2</sup>Institute of Geoecology, Technische Universität Braunschweig, 38106 Braunschweig, Germany

<sup>a</sup>present address: BASF Digital Farming GmbH, 50678 Cologne, Germany

**Correspondence:** Pia Gottschalk (pia.gottschalk@gfz-potsdam.de) and Torsten Sachs (torsten.sachs@gfz-potsdam.de)

Received: 11 December 2023 – Discussion started: 9 January 2024

Revised: 27 May 2024 – Accepted: 7 June 2024 – Published: 16 August 2024

**Abstract.** Improving the accuracy of monitoring cropland CO<sub>2</sub> exchange at heterogeneous spatial scales is of great importance for reducing spatial and temporal uncertainty in estimating terrestrial carbon (C) dynamics. In this study, an approach to estimate daily cropland C fluxes is developed and tested by combining time series of field-scale eddy covariance (EC) CO<sub>2</sub> flux data and Sentinel-2 satellite-based vegetation indices (VIs) after appropriately accounting for the spatial alignment between the two time series datasets. The study was carried out for an agricultural field (118 ha) in the lowlands of northeastern Germany. The ability of different VIs to estimate daily net ecosystem exchange (NEE) and gross primary productivity (GPP) based on linear regression models was assessed. Most VIs showed high (> 0.9) and statistically significant ( $p < 0.001$ ) correlations with GPP and NEE, although some VIs deviated from the seasonal pattern of CO<sub>2</sub> exchange. By contrast, correlations between ecosystem respiration (Reco) and VIs were weak and not statistically significant, and no attempt was made to estimate Reco from VIs. Linear regression models explained generally more than 80 % and 70 % of the variability in NEE and GPP, respectively, with high variability among the individual VIs. The performance in estimating daily C fluxes varied among VIs depending on the C flux component (NEE or GPP) and observation period. Root mean square error (RMSE) values ranged from 1.35 g C m<sup>-2</sup> d<sup>-1</sup> using the green normalized difference vegetation index (GNDVI) for NEE to 5 g C m<sup>-2</sup> d<sup>-1</sup> using the simple ratio (SR) for GPP. This equated to an underestimated net C uptake of only 41 g C m<sup>-2</sup> (18 %) and an overestimation of gross C uptake of 854 g C m<sup>-2</sup> (73 %). Differences between the measured

and estimated C fluxes were mainly explained by the diversion of the C flux and VI signal during winter when C uptake remained low, while VI values indicated an increased C uptake due to relatively high crop leaf area. Overall, the results exhibited similar error margins to mechanistic crop models. Thus, they indicated the suitability and expandability of the proposed approach for monitoring cropland C exchange with satellite-derived VIs.

## 1 Introduction

Managed cropland soils extend over 15.1–18.8 Mkm<sup>2</sup> (11.6 %–14.4 % of the global ice-free land area) (Luyssaert et al., 2014). They store about 131.81 Pg of organic carbon (C) in the first 30 cm of the soil profile (Zomer et al., 2017) and constitute about 10 % of the total terrestrial soil organic C stock (Jobbagy and Jackson, 2000). Cropland soils have historically lost a large amount of the original soil organic C (Guo and Gifford, 2002; Sanderman et al., 2017). This deficit, however, represents a large potential for sequestering C today and in the future (Lal et al., 2018; Zomer et al., 2017). Therefore, croplands have been identified as the most promising land use type to compensate for fossil fuel emissions (“4 per mille” initiative; Minasny et al., 2017; Rumpel et al., 2020). Whether cropland soils are a net C source or sink, however, is determined by the total cropland C balance. As opposed to natural ecosystems in which the net C balance is mainly determined by the balance between gross primary production (GPP) and ecosystem respiration (Reco) (Chapin et al., 2006) only, the cropland net ecosys-

tem C balance includes (lateral) C fluxes from harvest exports and manure imports (Ciais et al., 2010) and some minor C losses from C leaching, erosion, or fire. However, the atmospheric exchanges of CO<sub>2</sub> of croplands (GPP and Reco) are the two largest and most uncertain fluxes in the regional cropland carbon balance (Ciais et al., 2010). Regionally integrated estimates of GPP and Reco are difficult in highly diverse and geographically patchy croplands, which results in high uncertainty of spatially explicit estimates of cropland C stock changes (Pique et al., 2020). Robust knowledge and dedicated monitoring of the delicate balance between these two fluxes, however, are important for guiding climate change mitigation measures. Furthermore, mitigation measures based on cropland soil C sequestration require high accuracy of C flux estimates for monitoring, reporting, and verification purposes.

The state-of-the-art method for measuring ecosystem–atmosphere C exchanges is the eddy covariance (EC) method based on micrometeorological theory (Baldocchi, 2003). This method allows for direct net ecosystem exchange (NEE) measurements which integrate C dynamics of spatially highly variable soil organic carbon (SOC) stocks. Subsequent flux processing partitions NEE into GPP and Reco (Reichstein et al., 2005; Lasslop et al., 2010; Wutzler et al., 2018). Although results are robust and commonly accepted, they are confined to local, homogeneous footprint (FP) areas (Smith et al., 2010).

To assess and monitor the spatial variability of C fluxes at the local scale and across ecosystems, a global network of EC flux sites (FLUXNET) has been established of which, however, only 20 out of 212 sites (here, FLUXNET2015 Dataset) are cropland sites (Pastorello et al., 2020). They are thus sparse relative to the vast diversity of existing croplands. To overcome the spatial gap between local measurements from a limited number of sites and regional to global C exchange estimates, the combination of local EC data with remote sensing products such as satellite-derived vegetation indices (VIs) has been explored (Tramontana et al., 2016; Jung et al., 2011; Fu et al., 2014; Bazzi et al., 2024; Mahadevan et al., 2008; Xiao et al., 2008, 2010, 2011).

The light use efficiency (LUE) concept (Medlyn, 1998; Yuan et al., 2014) and the relationship of fractional absorbed photosynthetically active radiation (FPAR) with VIs (Myeni and Williams, 1994) allow VIs to be used as proxies for GPP (Running et al., 2004; Zhou et al., 2014). However, GPP is only one part of the C exchange, and for estimations of the full C budgets of the ecosystem, the net exchange of C fluxes (NEE) is required. Therefore, the correlation of GPP with Reco (Baldocchi, 2008; Baldocchi et al., 2015; Ma et al., 2016) can be leveraged to directly link VIs with NEE (Noumonvi et al., 2019; Wohlfahrt et al., 2010; X. Huang et al., 2019).

Interestingly, a direct correlation between GPP and VIs, rather than more complex approaches incorporating additional environmental drivers, can outperform LUE-type mod-

els such as the MODIS GPP (“MOD17”) product across ecosystems (Sims et al., 2006), particularly for croplands (X. Huang et al., 2019). The high variability in green biomass during the phenological cycle seems to make croplands especially suitable for directly tracking GPP with VIs, without the need to incorporate meteorological drivers (Tramontana et al., 2015). The latter is attributed to the variability in plant dynamics being determined rather by human interventions such as fertilizing, tilling, sowing, and harvest dates (Tramontana et al., 2016). The goal of optimizing specific plant performance locally can, to some extent, override environmental conditions. This raises the question of whether a simple relationship between VIs and NEE can provide sufficient accuracy for estimating C fluxes in croplands as opposed to more complex approaches.

While numerous studies assess the direct link of GPP with satellite-derived VIs (e.g., Badgley et al., 2017; X. Huang et al., 2019; Peng and Gitelson, 2012; Joiner et al., 2018; Liu et al., 2021; Rahman et al., 2005; Wang et al., 2004; Juszczak et al., 2018; Lin et al., 2019), the number of studies assessing the correlation of VIs with NEE is small (Olofsson et al., 2008; Noumonvi et al., 2019; Wohlfahrt et al., 2010; X. Huang et al., 2019; Sims et al., 2006), and to our knowledge there is no such study including or dedicated to croplands.

With the increasing availability of higher-resolution satellite imagery such as EnMAP, Sentinel-2C, and Landsat Next, the link between these data and field-scale C fluxes can provide greater spatial accuracy and requires further investigation. Except for the study by Madugundu et al. (2017), most studies exploring the potential of satellite-derived VIs to serve as proxies for estimating cropland C fluxes use MODIS or MODIS-like resolution products. Although the potential of finer-resolution satellite images such as Landsat or Sentinel-2 – as opposed to coarser, MODIS-like resolution – for cropland C flux estimates at spatial scales has been demonstrated (Gitelson et al., 2012; Fu et al., 2014; Wolanin et al., 2019; Bazzi et al., 2024; Madugundu et al., 2017; Chen et al., 2010; Spinosa et al., 2023; Pabon-Moreno et al., 2022), a direct link between VIs and cropland NEE has not been explored. All of these studies employ complex approaches (process-based models, machine learning) which demand high computational efforts and are heavy on auxiliary data requirements. Further, complex approaches always introduce additional sources of uncertainty – model structure and parameter uncertainty as well as input data uncertainty (Wattenbach et al., 2006) – and can be difficult to parameterize (Sims et al., 2006). Exploring a direct and straightforward link would clarify the explanatory power of VIs themselves, enabling systematic examination of the conditions under which additional data are truly necessary without undermining the comprehensive meaningfulness of the VIs. Furthermore, except for Bazzi et al. (2024) and Fu et al. (2014), all studies focus on GPP rather than on NEE, and most of the aforementioned studies explore only a few VIs.

Additionally, none of these studies are dedicated to examining the link between C fluxes and VIs along the phenological cycle at the plot scale, which is imperative for evaluating the robustness and accuracy of linking the two signals.

Another advantage of using finer-resolution imagery is the ability to match the spatial footprint of the two signals. Large-area products of C fluxes which combine remotely sensed VIs with EC-observed C dynamics (Jung et al., 2019) (the FLUXCOM initiative: <http://www.fluxcom.org/>, last access: 12 August 2024) can have a relatively low spatial resolution of 0.0833°. Such a coarse resolution can cause a systematic mismatch between the satellite sensor and the EC tower FP (Tramontana et al., 2016) and mostly does not distinguish individual agricultural fields well. To improve the estimation of C exchange for croplands, the need for higher-resolution remote sensing data such as Landsat has been pointed out (Tramontana et al., 2016). Furthermore, Kong et al. (2022) showed the superiority of FP-matched regression between GPP and high-resolution satellite near-infrared (NIR) maps over in situ (NIR sensor location) regressions for different cropping fields in California.

All of this highlights the need for and shows the promise of further investigating the capabilities of high-resolution satellite imageries in directly estimating carbon fluxes in croplands and monitoring them by a rigorous evaluation of comprehensive spectral indices derived from finer-resolution satellite imageries while appropriately leveraging EC-based C flux measurements.

The most commonly used VI in combination with NEE is the normalized difference vegetation index (NDVI), followed by the enhanced vegetation index (EVI) and the land surface water index (LSWI). Noumonvi et al. (2019) additionally used the green NDVI (GNDVI), the normalized difference surface water index (NDSWI), the soil-adjusted VI (SAVI), and the modified normalized difference water index (MNDWI). Wohlfahrt et al. (2010) use the simple ratio (SR) and Tramontana et al. (2016) the normalized difference water index (NDWI). However, only Tramontana et al. (2016) link VIs (NDVI, EVI, NDWI, and LSWI) to cropland NEE, GPP, and Reco, while the other studies assess their suitability for grassland C fluxes. Assuming the predictive performance of GPP from VIs for croplands also holds true for cropland NEE and Reco, our VI selection was based on the performance of VI for GPP estimation in croplands. In this regard, typical satellite-sensor-derivable VIs such as NDVI, EVI, EVI2, and SR (C. J. Huang et al., 2019a; Peng and Gitelson, 2012) indicate the highest potential for our study.

Here, we introduce a new agricultural EC measurement site in northeastern Germany and present daily and annual CO<sub>2</sub> dynamics over two and a half growing seasons along with the relevant site, meteorological, and management data. We explore the capacity of high-resolution satellite imagery in conjunction with a comprehensive range of VIs to estimate daily NEE, GPP, and Reco. To overcome the problem of the potential spatial mismatch of the two signals, the source

area of the two signals was matched to the same footprint area. Instead of average NEE values (e.g., midday or 8 d averages around acquisition dates), integrated daily NEE values were used to allow for continuous full-C-budget calculations. Challenges along the course of the phenological cycle were analyzed to better understand the achievable accuracy and uncertainties associated with this approach.

To summarize, the objectives of this paper were (1) to present and evaluate the CO<sub>2</sub> dynamics and C budgets of a newly established EC cropland site in northeastern Germany; (2) to assess the performance of a range of various high-resolution imagery-derived VIs to estimate daily NEE, GPP, and Reco at this site; and (3) to discuss and evaluate the results of this simple approach in comparison with more complex methods and future research requirements.

## 2 Data and methods

### 2.1 Site description

The net ecosystem exchange is measured with an eddy covariance (EC) system located in an arable field in the northeastern lowlands of Germany (53°52′05.7″ N, 13°16′07.0″ E) southeast of the village of Heydenhof (Fig. 1). The site is situated in an Upper Pleistocene landscape with a temperate oceanic climate of yearly mean temperature and precipitation of 8 °C and 580 mm during 1961–1990 and 9.2 °C and 575 mm during 1991–2020, respectively (nearby German Weather Service climate stations “Anklam” and “Greifswald”). The soil is a clayey loam with more than 10 % clay and contains about 1.5 %–2 % organic C with a high gradient across the field (personal communication with land manager, Mortimer von Maltzahn, 19 January 2022). The continuous half-hourly and ongoing EC measurements started on 4 March 2020, 17:30 UTC, at a measurement height of 7 m above ground level. The site has been under arable cropping for at least 60 years, with a crop rotation of 1/3 winter rape (WR) and 2/3 winter wheat (WW) during the past few years (personal communication with land manager, Mortimer von Maltzahn, 19 January 2022). The details of the crop rotation and management for the time and field under investigation surrounding the EC tower (named “main field” here) is outlined in Table 1. Exact dates of management were not provided by the land manager and were delineated from visual inspection of half-hourly imagery provided by a tower-mounted camera overlooking the field facing northwards.

The EC tower is situated close to the border of an adjacent field to the east (distance: 120 m) and relatively close to an adjacent field to the south (distance: 285 m) (Fig. 1). The tower itself sits on the southern edge of a dry cattle hole (north–south length 45 m, width 25) at an altitude of 22.7 m above sea level.

**Table 1.** Crop management information for the main field. Note that information about yield and straw amounts as well as crop and soil management is based on long-term averages. Yearly field-scale data are confidential to the farmer.

Season	2019/2020	2020/2021	2021/2022
Crop	winter rape	winter wheat	winter wheat
Sowing date	approx. 12 Aug to 25 Aug	approx. 15 Sep to 15 Oct	14 Oct 2021
Harvest date	23 Jul 2020	9 Aug 2021	21 Jul 2022
Yield [ $\text{t C ha}^{-1}$ ]	1.8	4.05	4.05
Straw [ $\text{t C ha}^{-1}$ ]		1.92 (left in the field)	1.92 (removed)
Fertilizer [ $\text{kg N ha}^{-1}$ ]	100 (cattle manure in autumn) +140 (urea in spring)	220 (urea in spring)	220 (urea in spring), partly replaced by organic fert.
Soil cultivation/plowing	3× between harvest and sowing	3× between harvest and sowing	3× between harvest and sowing
Herbicides/pesticides	3–4× in spring	4× in spring	4× in spring

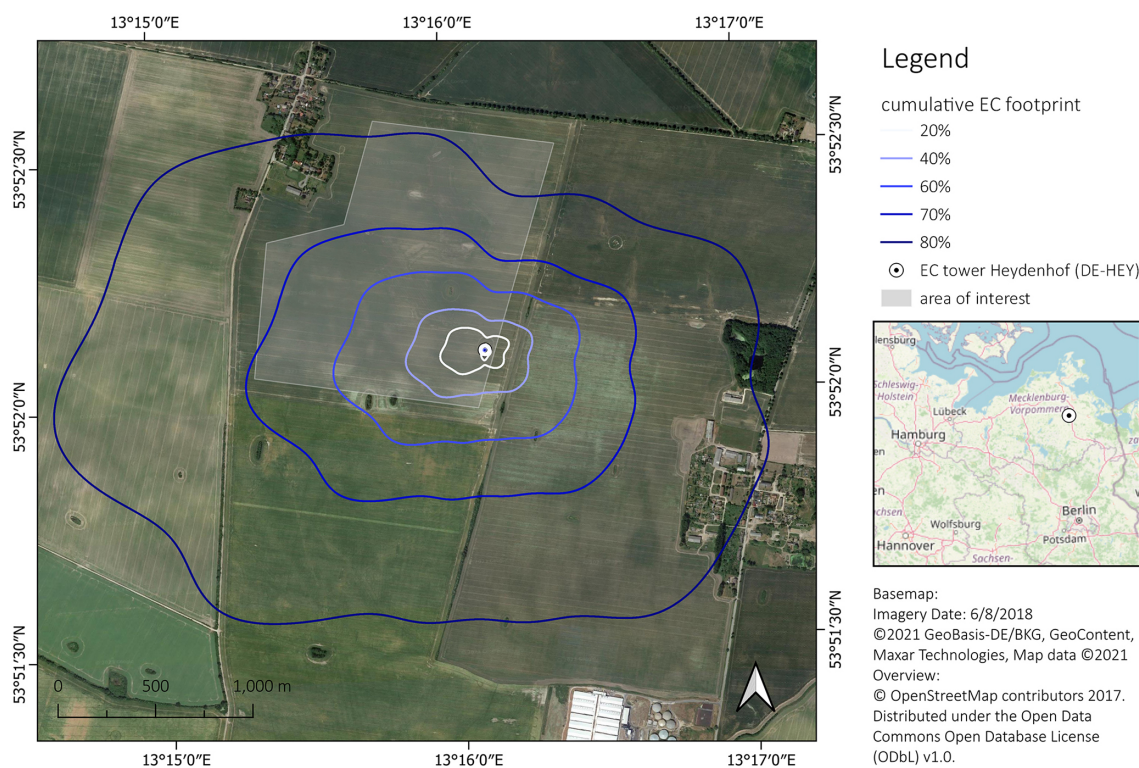


**Figure 1.** Setting and layout of the arable fields surrounding the EC tower in northeastern Germany. Isolines denote the cumulative contribution of the source area to the flux signal over the measurement period (5 March 2020 to 23 August 2022) of the “Heydenhof” EC tower. For more detailed information of the cumulative source area, please refer to Appendix B. The transparent gray area outlines the polygon for which average satellite-derived vegetation indices were calculated. The outer borders of the respective field (as seen on the picture) surround the area for which the homogeneous (in terms of crop dynamics) EC flux time series is calculated (main field; see text). (Original map designed by Karl Kemper.)

## 2.2 Measurement equipment and raw flux data processing

EC flux measurements were carried out with a 3D ultrasonic anemometer (HS-50, Gill Instruments, UK) and an open-path infrared gas analyzer (LI-7500DS, LI-COR Biosciences, USA). Data from these sensors were measured

with a frequency of 20 Hz. Half-hourly fluxes were calculated with the software EddyPro (version 7.0.7, LI-COR Biosciences, USA). Meteorological data including air temperature and relative humidity (HMP155, Vaisala, FI), barometric pressure (model 61302V, Young, USA), and incoming and outgoing shortwave and infrared radiation (CNR4, Kipp & Zonen, NL) and photon flux density (LI-190, LI-COR Bio-

sciences, USA) were measured with a frequency of 1 Hz and averaged to half-hourly values. The 15 min precipitation data were collected with an RG Pro Adcon Rain Gauge (Itzerott et al., 2018).

### 2.3 EC data processing

The handling of half-hourly NEE data, from 5 March 2020 to 23 August 2022, followed standard EC data processing steps and is further detailed in Appendix A–C. Data were quality-controlled (Appendix A) and filtered for spatial representation of the main field by footprint modeling (Appendix B). The FP filter threshold was optimized according to data availability (i.e., acceptable number of gaps) and representativeness of the main field. Times of insufficient turbulence were filtered by the  $u^*$ -threshold approach (Appendix C), and subsequent gap filling (Appendix C) used only data of the highest quality, i.e., quality flag = 0 following the CarboEurope IP flag convention (Mauder and Foken, 2004). Flux partitioning into GPP and Reco followed Reichstein et al. (2005).

Half-hourly C fluxes were subsequently aggregated to daily sums for linking with satellite data. General data processing, analysis, and visualization were carried out in R (R Core Team, 2021). NEE sign notation followed the micrometeorological sign convention, which denotes C gains by vegetation with negative values and C losses to the atmosphere from auto- and heterotrophic respiration with positive values (Aubinet et al., 2009). When describing and discussing C fluxes in the text, NEE and GPP are referred to by their absolute values such that NEE and GPP “decrease” with a decrease in C uptake.

### 2.4 C budget calculation and evaluation

To assess the magnitude of the C exchange as compared with the other components of the cropland soil C budget, a simplified C budget (A4) for the two WW growing seasons (sowing to harvest, Table 1) was calculated as follows:

$$\text{C budget} = \text{NEE} - \text{import} + \text{export},$$

where import is limited to the C of seeds, since no manure is applied, and export refers to C harvest losses.

### 2.5 Satellite-based vegetation indices

Average values of VIs (Table 2) of satellite imagery pixels were calculated from within the borders of the main field (transparent polygon in Fig. 1). The source area of the satellite signal thus matches the source area of the EC tower. The L2A products of the Sentinel-2 multi-spectral instrument provided by the Copernicus program of the EU and the European Space Agency were used. Sentinel-2 image processing was carried out on the Google Earth Engine platform (Gorelick et al., 2017). The quality map SCL (scene classification) of the Sentinel-2 L2A product is used to filter cloud, cloud shadow, and saturated pixels to ensure only

high-quality scenes were selected for the calculation of the vegetation indices. Satellite overpass time is approximately 10:00 (local solar time) for Heydenhof.

A continuous time series of daily satellite data was constructed by linear interpolation for the days between acquisition dates.

### 2.6 Correlation between daily C fluxes and vegetation indices

Correlations and linear regressions between daily C fluxes and VIs were calculated for the days on which reliable satellite data were available. The correlation was used to identify which VIs were most suitable for estimating C fluxes. Higher correlations indicate a higher coincidence and thus higher suitability of a VI to estimate C fluxes.

### 2.7 Estimation and evaluation of daily C fluxes from VIs by linear regression

Simple linear regressions of the type

$$\text{C flux} = a \times \text{VI} + b \quad (1)$$

were fitted to the 73 data pairs to subsequently estimate daily C flux values from interpolated satellite data. Resulting linear regressions were tested for statistical significance, and the coefficient of determination ( $R^2$ ) indicates the amount of variability in the dependent variable (i.e., C flux) explained by the regression.

As a measure of accuracy for the final estimation of daily C fluxes (902 data points), the correlation coefficient  $\rho$  was used for association (trend similarity) and the  $R^2$  and RMSE for coincidence, i.e., percentage variability explained by the regression and total difference between measured and estimated value, respectively. Additionally, the “model efficiency” factor  $E$  (Nash and Sutcliffe, 1970) was calculated to characterize the ability of the linear models to replicate daily C fluxes. Values range from  $-\infty$  to 1, where 1 indicates a near-perfect fit, 0 denotes that the approach is not better than taking the mean of the observations, and any value below 0 rates the estimation approach as poor.

Linear models were set up for three different evaluation periods: (1) the whole observation period ranging from the first to last satellite image, (2) for the two WW growing periods ranging each from sowing to harvest, and (3) for the first WW growing period (WW1). The last one was subsequently used to estimate daily C fluxes of the second WW growing period (WW2) as an evaluation of the temporal transferability of this approach and associated absolute errors. Our linear-regression-based WW2 C flux estimates were subsequently evaluated by comparing our results with simulation results of mechanistic crop models and with satellite data–model fusion approaches estimating cropland C fluxes at various (other) sites.

**Table 2.** List of vegetation indices calculated from Sentinel-2. BLUE, GREEN, RED, RE1–3 (red edge), NIR (near-infrared), and SWIR (shortwave infrared) refer to the respective spectral bands of Sentinel-2 (B2–B7, B8A, B11).

Index	Formula	Name, range, purpose
NDVI	$(\text{NIR} - \text{RED}) / (\text{NIR} + \text{RED})$	<i>Normalized difference vegetation index.</i> This characterizes the density/green biomass of vegetation (Rouse et al., 1974).
EVI	$2.5 \times ((\text{NIR} - \text{RED}) / (\text{NIR} + 6 \times \text{RED} - 7.5 \times \text{BLUE} + 1))$	<i>Enhanced vegetation index.</i> This reduces soil and atmospheric contamination of vegetation signals and optimizes the vegetation signal in areas with a high leaf area index (LAI) where NDVI would saturate (Liu and Huete, 1995).
EVI2	$2.5 \times ((\text{NIR} - \text{RED}) / (\text{NIR} + 2.4 \times \text{RED} + 1))$	<i>2-band enhanced vegetation index.</i> This has the highest similarity with the EVI but without using the blue band at which surface reflectance values can be sensitive to residual errors in atmospheric correction (Jiang et al., 2008).
GNDVI (i.e., $-\text{NDWI}_{\text{McFeeters}}$ )	$(\text{NIR} - \text{GREEN}) / (\text{NIR} + \text{GREEN})$	<i>Green NDVI.</i> This is an indicator of the photosynthetic activity of vegetation assessing the moisture content and nitrogen concentration in plant leaves; it is more sensitive to chlorophyll concentration than NDVI (Gitelson et al., 1996). The GNDVI is the inverse of the NDWI as defined by McFeeters (1996).
NDSVI	$(\text{SWIR1} - \text{RED}) / (\text{SWIR1} + \text{RED})$	<i>Senescence index (0–1).</i> This detects senescent vegetation (Qi et al., 2002).
NDWI (or LSWI)	$(\text{NIR} - \text{SWIR1}) / (\text{NIR} + \text{SWIR1})$	<i>Normalized difference water index/land surface water index (–1 to 1).</i> This is used to monitor changes in the water content of leaves; it should be used as complementary to NDVI and not to substitute it (Chandrasekar et al., 2010; Gao, 1996).
MNDWI	$(\text{GREEN} - \text{SWIR1}) / (\text{GREEN} + \text{SWIR1})$	<i>Modified normalized difference water index.</i> This is modified from $\text{NDWI}_{\text{McFeeters}}$ to enhance open water features (Xu, 2006).
SAVI	$((\text{NIR} - \text{RED}) / (\text{NIR} + \text{RED} + L)) \times (1 + L)$ , where $L = 0.5$	<i>Soil-adjusted vegetation index.</i> This transformation of NDVI nearly eliminates soil-induced variations in the VI (Huete, 1988).
SR	$\text{NIR} / \text{RED}$	<i>Simple ratio.</i> Leaves absorb more red than infrared light; thus, the ratio increases with more green biomass (Jordan, 1969).
S2REP	$705 + 35 \times (((\text{RE3} + \text{RED}) / 2) - \text{RE1}) / (\text{RE2} - \text{RE1})$	<i>Sentinel-2 red-edge position (REP).</i> REP is the point of the maximum slope along the red edge (RE); it has been used to enhance estimates of leaf and canopy chlorophyll content (Frampton et al., 2013; Guyot and Baret, 1988).

### 3 Results and discussion

#### 3.1 Evaluation of C exchange dynamics and C budgets

In total, 902 d of half-hourly flux data contributed to this analysis. Since only measurements of the highest quality were kept for subsequent processing (see Sect. 2.3), only

44 % of half-hourly data were available for further processing.

This was further reduced by the integration of the FP model results. Filtering the dataset for the main field (FP modeling) reduced the available “qc0 data” to 18.7 % and 12.8 % for an FP filter threshold of 0.7 and 0.8, respectively. The higher threshold renders very long and continuous gaps



during winter, which makes the gap filling highly uncertain and was the main reason for the deviations between the two gap-filled time series using 0.7 or 0.8 as the threshold for FP filtering (data not shown). While using the FP model threshold of 0.8 valid fluxes might have been more representative for the main field, the time series employing the threshold of 0.7 was concluded to be more reliable and good at balancing the loss of some representativeness. Still, the available data coverage was quite low compared to other studies (Schmidt et al., 2012). The proportion of missing data is higher during the nighttime (defined as fluxes at  $< 20 \text{ W m}^{-2}$  global radiation) than during the daytime, i.e., 93 % versus 70 %, respectively (for the threshold of 0.7).

The final time series was gap-filled using a single  $u^*$  threshold of 0.2 as estimated by REddyProc (Wutzler et al., 2018). The large proportion of gaps did not allow for season-specific  $u^*$ -threshold estimation. Moureaux et al. (2008) also used a single value for a WW crop in Belgium, which was very similar to ours, i.e., 0.22. They further suggested that  $u^*$  uncertainty had a very low impact on fluxes. Figure 2 depicts the gap-filled NEE, GPP, and Reco curves along with relevant meteorological variables.

Generally, growing conditions were more favorable in the second growing season than in the first and last (see “climate growing season” parameters in Fig. 2), which was reflected in the higher absolute values of all fluxes in 2021 than in 2020 and 2022. Overall, NEE, GPP, and Reco flux dynamics at our cropland site showed a typical pattern of European WR and WW cropping. An in-depth description of C flux dynamics at our cropland site is presented in the Supplement.

The total C budget during the observation period amounted to a total loss of  $4.46 \text{ t C ha}^{-1}$ , accounting for C exports through WR and WW harvests and straw removal after the last harvest, ignoring C import via seeds. However, C import via seeds typically ranges between 0.02 and  $0.08 \text{ t C ha}^{-1}$  for WW (Aubinet et al., 2009; Schmidt et al., 2012; Waldo et al., 2016), which is negligible compared with the other C budget components. C export through harvest and straw removal amounts to  $11.82 \text{ t C ha}^{-1}$ . C losses from the systems thus outbalance the total net uptake of  $-7.36 \text{ t C ha}^{-1}$ . Uncertainty as provided by the  $u^*$ -bootstrapping procedure of REddyProc ranged from  $-7.53 \text{ t C ha}^{-1}$  (0.05 percentile) to  $-7.37 \text{ t C ha}^{-1}$  (0.95 percentile) for the net atmospheric C exchange. The C budget of the two individual WW seasons amounted to a net C uptake in 2020/2021 of  $-1.34 \text{ t C ha}^{-1}$  and to a net C loss in 2021/2022 of  $3.68 \text{ t C ha}^{-1}$  due to the removal of straw. They were well within the range of respective C budgets of European WW sites, ranging from  $-4.45$  to  $2.54 \text{ t C ha}^{-1}$  (Waldo et al., 2016; Anthoni et al., 2004; Aubinet et al., 2009; Béziat et al., 2009; Li et al., 2006; Schmidt et al., 2012; Wang et al., 2015). Individual C budget components are reported in Table 3.

### 3.2 Satellite vegetation indices

In total, 73 scenes with good-quality surface reflectance data were obtained for our main field for the period 5 March 2020 to 23 August 2022. Standard deviations of VIs within the main field per image were small, indicating low spectral heterogeneity of the main field, and were thus considered negligible for the purpose of this study (Fig. 3).

The temporal dynamics of satellite-derived VIs generally matched well with the seasonal pattern of NEE and GPP (Fig. 3) – except for NDSVI and MNDWI, where an increase in absolute VI values concurred with an increase in absolute NEE and GPP values. One marked deviation occurred during the onset of the winter seasons, which coincided with longer gaps in satellite images (winter months are generally characterized by higher cloud cover causing gaps in satellite imagery time series). Here, the gap in winter VI data was characterized by a presumably initial increase in absolute VI values without indication of a maximum and by relatively high absolute VI values at the onset of spring in the following year. However, a respective dynamic (increase in absolute GPP or NEE) could not be observed. GPP values showed low C uptake (about  $-1 \text{ g C m}^{-2} \text{ d}^{-1}$ ) from October to February, while net C uptake increased only slightly (due to decreasing Reco). The increase in absolute VI values toward the end of the years 2020 and 2021 for WW, which is not common (Itzerott and Kaden, 2006a, b), was observed at our site in the years prior to our study period as well (data not shown). Similar patterns were also observed for WW in Kansas, USA (Masiale et al., 2010), and an immediate increase in “greenness” after crop emergence was also corroborated by the “Greenness Index” of the PhenoCam pictures of Heydenhof ([https://phenocam.nau.edu/webcam/roi/heydenhof/AG\\_1000/](https://phenocam.nau.edu/webcam/roi/heydenhof/AG_1000/), last access: 12 August 2024). It was thus hypothesized that the diversion between the NEE and GPP signals and the VI signals can be explained in analogy to the phenological development of winter crops. After emergence, the plants quickly developed a relatively high leaf area index (LAI) with a high specific leaf area ( $\text{cm}^2 \text{ g}^{-1}$ ) before winter dormancy. They assimilated less C into biomass (i.e., GPP) per leaf area than during the warmer part of the growing season (Korres et al., 2014; Van Oosterom and Acevedo, 1993; Weaver et al., 1994). Under light-limiting conditions, plants invest in leaf area rather than leaf biomass (Rawson et al., 1987). This presumably caused the mismatch between the course of GPP and NEE and the VIs. This winter deviation counteracted the straightforward linear correlation which was noted for the rest of the observation period. It denoted a systematic discrepancy in the linear relationship between VIs and GPP and NEE.

It should be noted, however, that Sentinel-2 VIs were able to pick up the decline in NEE and GPP during WR flowering (from around 23 April to around 27 May 2020). The sensitivity of VIs to WR flowering has also been reported by Itzerott and Kaden (2006b) for NDVI.

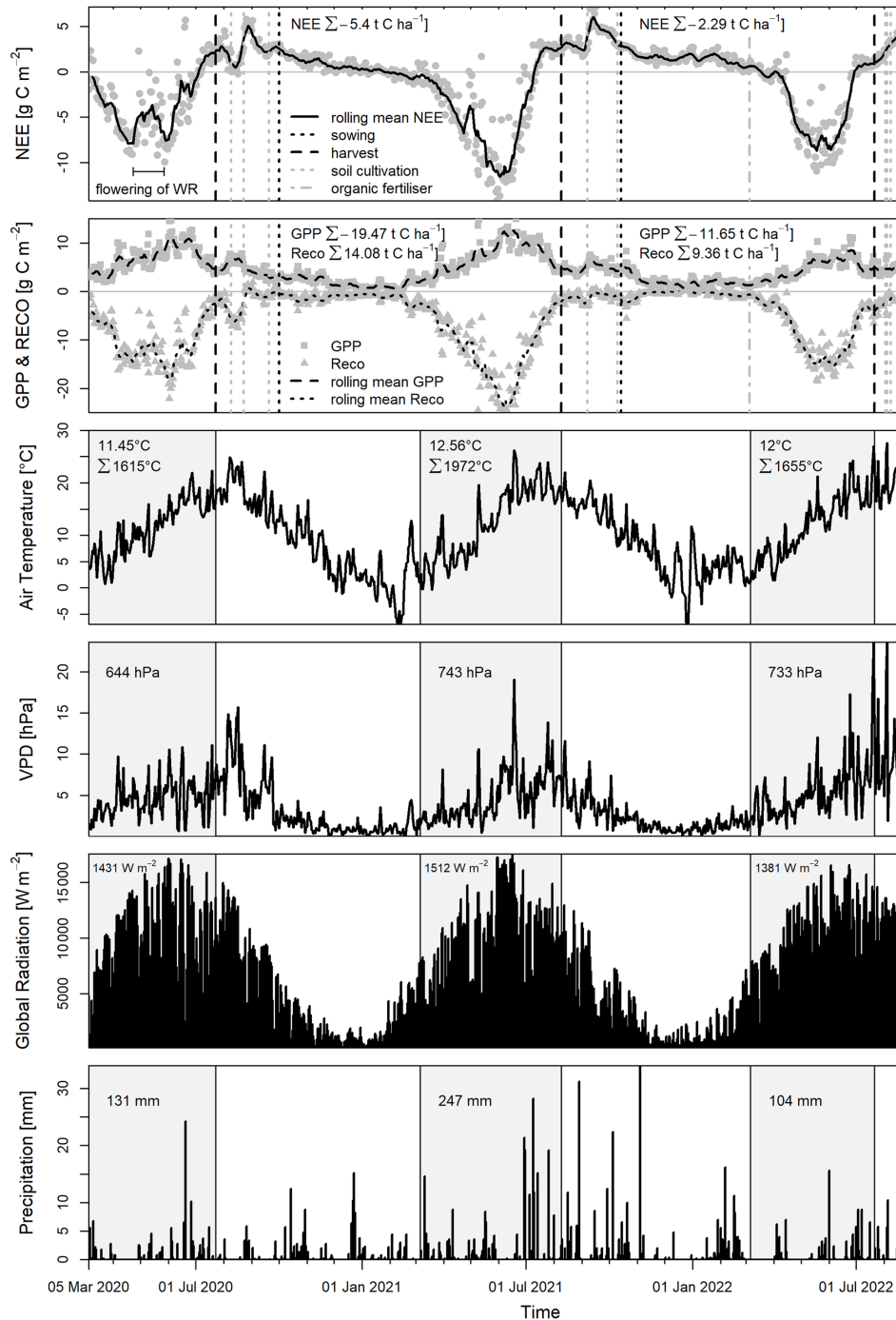


**Figure 2.** Gap-filled time series of daily sums of NEE (gray dots), GPP (gray squares), and Reco (gray triangles) [ $\text{g C m}^{-2} \text{ d}^{-1}$ ]; 10 d rolling means of NEE (solid black line in top panel), GPP (dashed black line), and Reco (dotted black line); and auxiliary meteorological variables (daily mean air temperature [ $^{\circ}\text{C}$ ], daily mean vapor pressure deficit (VPD) [hPa], daily sum of global radiation (Rg) [ $\text{W m}^{-2}$ ], daily sum of precipitation [mm]). Numbers in the C flux panels denote the seasonal (sowing to harvest) cumulative C fluxes. “Flowering of WR” in the top panel illustrates the duration of the flowering of winter rape (WR) from 23 April to 27 May. Gray boxes in the meteorological data panels denote the time period of the “climate growing season” for which descriptive climate parameters were calculated. They start on 5 March each year to match the first growing season in which EC measurements only started on 5 March 2020. They end on the days of harvest each year: 23 July 2020, 9 August 2021, and 21 July 2022. Dates for field management actions were determined from the inspection of tower-mounted field camera photos, since the respective information was not given by the farmer. Numbers in the gray boxes denote mean air temperature, temperature sums with base temperature 0, sum of VPD, Rg, and precipitation for the climate growing seasons, respectively.



**Table 3.** C budget components for the two WW growing seasons. Sums of C fluxes from sowing to harvest are reported in t C ha<sup>-1</sup>. Values in brackets denote the 0.05 and 0.95 percentile from the uncertainty estimation based on bootstrapping (Wutzler et al., 2018).

WW	NEE	GPP	Reco	Harvest	Straw	C budget
2020/2021	-5.4 (-5.47 to -5.34)	-19.47 (-19.44 to -18.63)	14.08 (13.17–14.1)	4.05	–	-1.34 (-1.42 to -1.29)
2021/2022	-2.29 (-2.292 to -2.3)	-11.65 (-11.68 to -11.35)	9.36 (9.05–9.38)	4.05	1.92	3.68 (3.67–3.68)

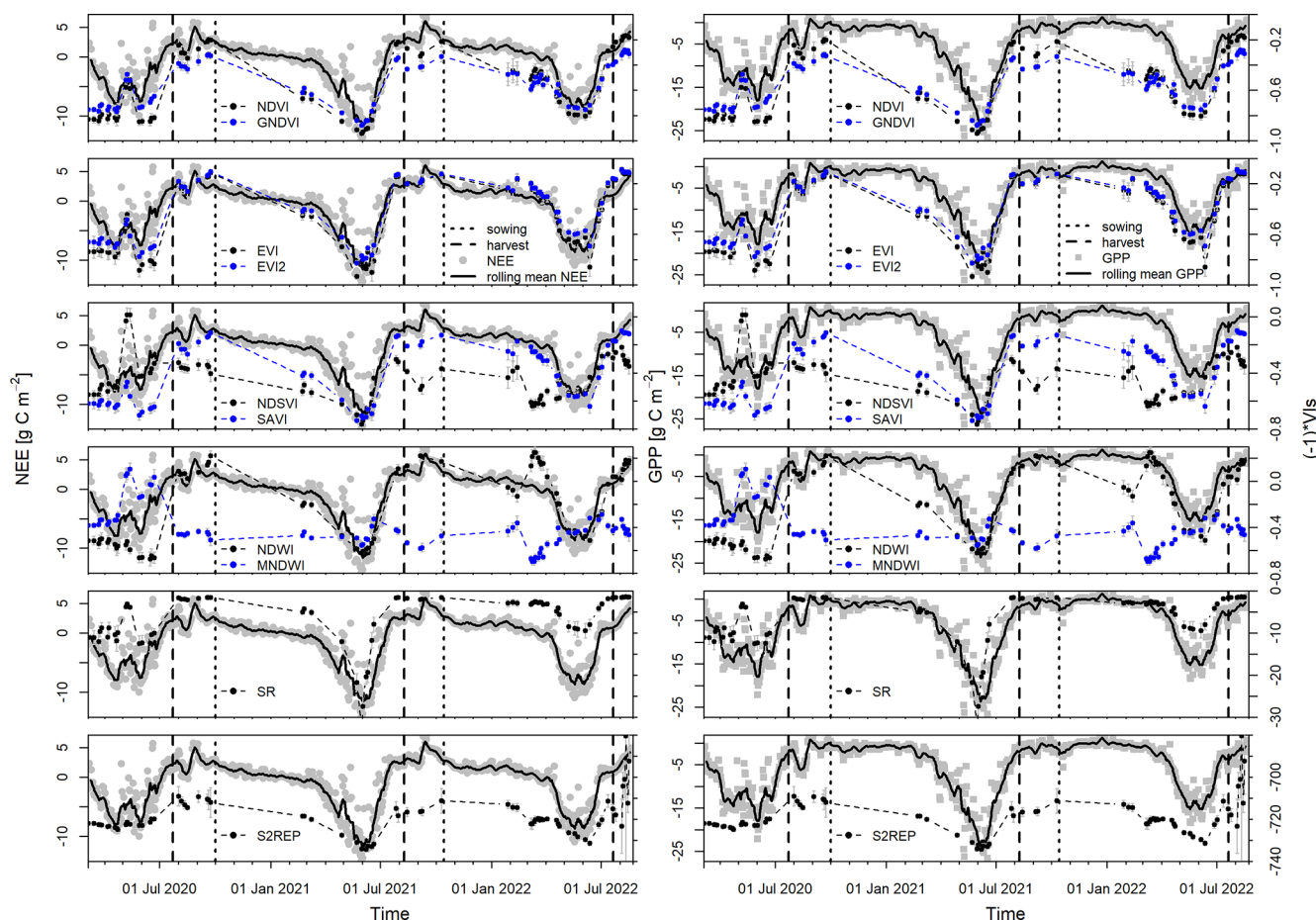


**Figure 3.** Course of NEE (gray dots) and GPP (gray squares) plotted against Sentinel-2-derived vegetation indices. C flux measurements are aggregated to daily sums superimposed with a 10 d rolling mean (black curves). Note that vegetation indices (black and blue dots) are plotted inversely to facilitate the comparison of the dynamic pattern of the two types of signals. Error bars (gray) of VIs indicate the standard deviation across the main field. Dashed black and blue lines connect the individual VIs to facilitate visually the course of VIs over time.

A less obvious deviation seemed to occur during senescence of WR. While the VI signals of NDVI, GNDVI, EVI, EVI2, SAVI, and NDSVI pick up the senescence-related drop in NEE for WW immediately, these VIs lag about 18 d (average across VIs based on the observation that VI values had reached a plateau at the same time as max C uptake (i.e., min NEE) and did not drop at the same time as NEE decreased; another similarly high VI value is observed about 18 d later

before the next VI value is much lower) behind the NEE signal for the senescence period of WR.

Most VIs were sensitive to the distinctly different C uptake dynamics of the summers of 2021 and 2022. C uptake is lower in 2022, and most VIs, except S2REP, MNDWI, and NDSVI, reach different levels of maximum absolute values.

### 3.3 Correlations between daily C fluxes and vegetation indices

Since the 73 data points of NEE, GPP, and Reco were not normally distributed (Shapiro–Wilk normality test,  $p < 0.05$ ), the non-parametric Spearman's rank correlation coefficient  $\rho$  was used to determine linear correlations. The linear correlations (Spearman's  $\rho$ ) and respective significance levels among C fluxes and VIs were generally high and significant for NEE and GPP but low and less significant for Reco (Fig. 4). Correlations among NEE, GPP, and Reco were all significant ( $p < 0.001$ ). GPP and Reco as well as GPP and NEE had  $\rho$  values of  $-0.8$  and  $0.88$ , respectively. Baldocchi (2008) and Baldocchi et al. (2015) reported correlations between GPP and Reco across ecosystems of  $0.89$  and  $-0.83$ , respectively. Please note that Baldocchi (2008) reports GPP (“ $F_A$ ”) with a positive sign and not with a negative sign as we do and as Baldocchi et al. (2015) do. Thus, his correlation value between GPP and Reco is positive as opposed to ours and to that of Baldocchi et al. (2015). The correlations can still be compared based on the absolute values. NEE and Reco correlated by  $-0.47$  only.

There was a highly significant correlation of NEE and GPP ( $p < 0.001$ ) with all VIs except MNDWI, which showed a lower level of significance ( $p < 0.01$ ). There was a highly significant correlation of GPP ( $p < 0.001$ ) with all VIs except MNDWI ( $p < 0.01$ ) and NDSVI ( $p < 0.05$ ), and both correlations showed a lower level of statistical significance. NEE correlated best with EVI2 and SAVI ( $\rho = -0.93$ ), followed by EVI, NDVI, GNDVI, SR ( $\rho = -0.92$ ), and S2REP ( $\rho = -0.9$ ), while NDWI showed a  $\rho$  value of  $-0.82$ . NDSVI and MNDWI had lower correlations of  $-0.51$  and  $-0.23$  only. GPP generally showed lower correlations with VIs and a different ranking in the following order: EVI, EVI2, and SAVI with a  $\rho$  value of  $-0.84$ , followed by NDWI ( $-0.83$ ), S2REP ( $-0.81$ ), NDVI ( $-0.8$ ), SR ( $-0.79$ ), and GNDVI ( $-0.77$ ) and then MNDWI and NDSVI with  $-0.38$  and  $-0.26$ , respectively. Reco showed significant but lower correlations with VIs except NDSVI, which showed no significant correlation. The highest correlation was observed for NDWI with  $0.58$  followed by S2REP with  $0.5$  and EVI, EVI2, and SAVI with  $0.47$ . The low correlation between Reco and VIs was not surprising, however, because respiration and its underlying auto- and heterotrophic processes are not directly connected with any surface reflectance characteristics (Wohlfahrt et al., 2010). While autotrophic respiration is closely linked with crop productivity (GPP) (Suleau et al., 2011) and has been shown to dominate total Reco in cropland systems during the growing season (60%–90%) (Suleau et al., 2011; Zhang et al., 2013), the processes and environmental factors governing heterotrophic processes are more complex (Grace et al., 2007) and not yet fully understood. While temperature had low explanatory power for autotrophic respiration, it is a strong driver of heterotrophic respiration (Suleau et al., 2011), which can dominate total Reco on an

annual basis (Zhang et al., 2013). The other main factor influencing heterotrophic respiration rates is the availability of organic substrate, while soil moisture might have a negligible impact in this context when soil water content is between wilting point and field capacity (Zhang et al., 2013). We speculate that the low correlation between Reco and VIs is mainly due to the heterotrophic component of Reco. Additional information on temperature and soil organic matter content could contribute toward improving this simple approach, although data availability for separating heterotrophic and autotrophic respiration might be a limiting factor.

A correlation analysis using data points from the WW growing periods solely indicated very similar correlations, which varied only by  $0.1$  or  $0.2$ , but the overall pattern stayed the same (data not shown). Additionally, when running the correlation analysis using only half-hourly flux data for the time of satellite overpass, i.e., flux data of 10:00–10:30 UTC, the correlations of C fluxes with satellite VIs slightly decreased in correlation intensity, but again the overall pattern and significance levels stayed the same (data not shown). This supported the applicability of daily accumulated fluxes for the approach presented here, as the aim was to estimate total C exchange over time.

Similarly high and significant correlations had been found between VIs and daily GPP/NEE for grasslands (Noumonvi et al., 2019; Wohlfahrt et al., 2010) and between VIs and daily GPP for WW crops (Juszczak et al., 2018). Noumonvi et al. (2019) also showed a lower correlation of NDSVI with NEE and GPP as compared with other VIs. While the correlations between VIs and daily GPP were found to be generally higher than with NEE for grasslands in previous studies (Noumonvi et al., 2019; Wohlfahrt et al., 2010), as opposed to our results for croplands, Noumonvi et al. (2019) showed that the correlations with NEE during dry phases were higher than with GPP for nearly all the VIs tested. Their definition of “dry phase” ( $VPD > 1500$  Pa), however, did not apply to the weather conditions of our site for the time of observation. Further investigations are needed to understand the causes of the differences in the efficacy of VIs to estimate GPP versus NEE and the impact of dry/wet conditions on the efficacy. Generally, our correlations for NEE and GPP were high compared with the correlation of VIs with other crop vegetation parameters such as biomass, LAI, chlorophyll *a* and *b*, or total nitrogen content (Boegh et al., 2002; Lilienthal, 2014), which are common parameters inferred from VIs for crop growth monitoring.

Overall, VIs based on the red, green, NIR, or red-edge spectral bands of the satellite sensors, such as NDVI, GNDVI, EVI, EVI2, SAVI, and SR, showed better correlations with NEE than VIs containing shortwave infrared (SWIR) band information, such as NDSVI, NDWI, and MNDWI. This did not hold true for correlations between VIs and GPP, where NDWI showed the second-highest correlation with GPP. Reco even correlated best with NDWI. VIs using red, green, NIR, or red-edge spectral bands were de-

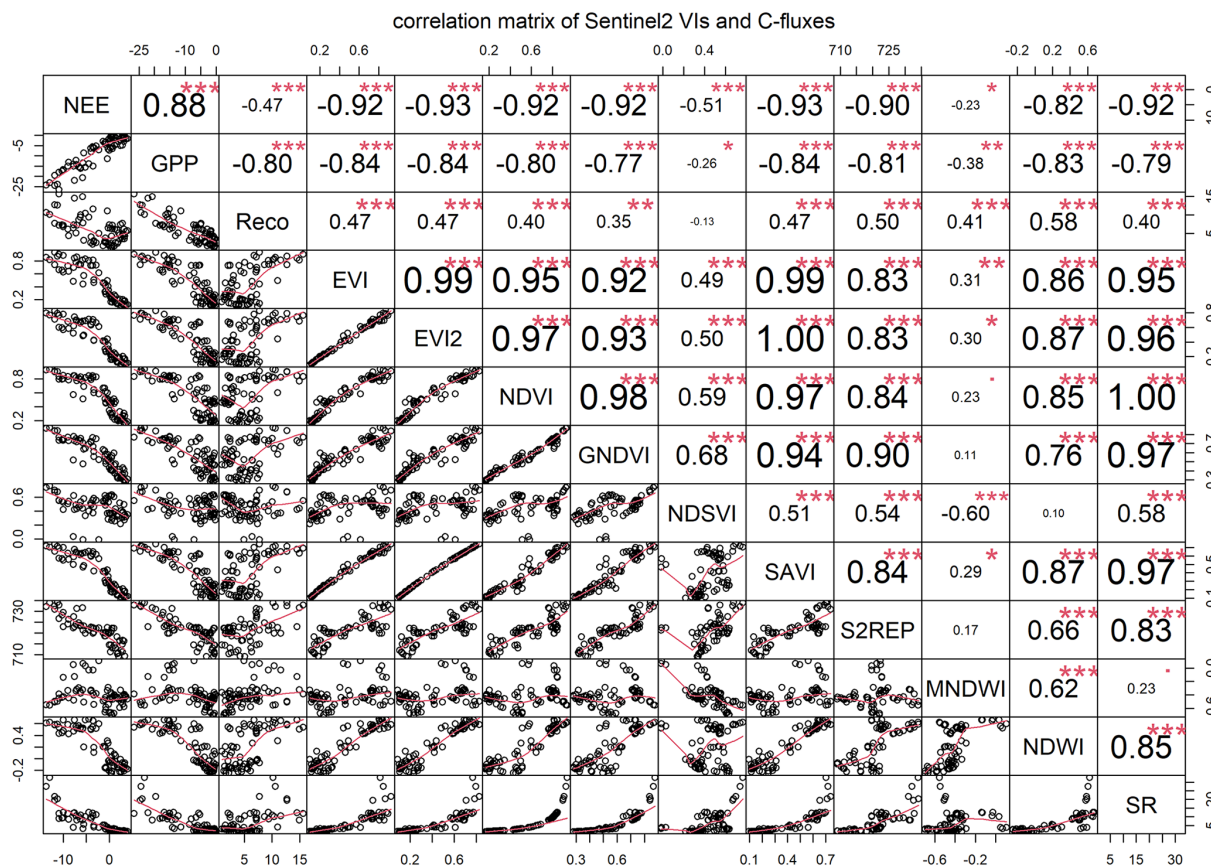


**Figure 4.** Rank correlation matrix of NEE, GPP, and Reco with EVI, EVI2, NDVI, GNDVI, NDSVI, SAVI, S2REP, MNDWI, NDWI, and SR from Sentinel-2. Numbers indicate the correlation coefficient  $\rho$ ; the size of the number is scaled by the degree of correlation. Red stars denote the statistical significance levels: \*\*\*  $p < 0.001$ , \*\*  $p < 0.01$ , \*  $p < 0.05$ , ·  $< 0.1$ , and “ ”  $< 1$ . Scatterplots display a fitted line (red).

veloped and are extensively used to evaluate the “greenness” or photosynthetic activity of plants. It was thus surprising that VIs correlated better with the NEE signal than with GPP, which is more directly related to photosynthetic plant activity, while NEE is composed of the two opposing fluxes of GPP and Reco.

### 3.4 Linear models to estimate daily C fluxes

For the linear modeling, the analyses were confined to NEE and GPP, since correlations between VIs and Reco were comparably low and Reco could also be calculated by deducting GPP from NEE. The curved relationship of NEE and GPP with VIs required a data transformation. EVI2 was chosen to determine the type of transformation because EVI2 showed one of the highest correlations with NEE (Fig. 4). Here, transforming NEE values to  $\log(-\text{NEE}+10)$  gave the best linear regression between EVI2 and NEE ( $R^2 = 0.86$ ,  $p < 0.001$ , residual standard error = 0.14). GPP values were transformed likewise with  $\log(\text{GPP}+10)$  ( $R^2 = 0.78$ ,  $p < 0.001$ , residual standard error = 0.18).

Interception and slope parameters as well as the coefficient of determination ( $R^2$  value) of VIs and NEE data were all statistically significant at the level of  $p < 0.001$  (Table 4).

Linear regressions explained on average 81 % of the variability in observed daily NEE values for the whole observation period, ranging from 65 % for SR to 87 % for EVI2 and SAVI. Linear regressions for the two WW growing periods showed higher explanatory power, with an average  $R^2$  value of 0.84, and, again, EVI2 and SAVI had the highest explanatory power as with the whole observation period with an  $R^2$  value of 0.91. For the first WW growing period only (WW1), linear regressions explained on average 92 %, ranging from 77 % for SR to 96 % for EVI2 and NDWI. For the second WW growing period (WW2), linear regressions explained on average 81 %, ranging from 62 % for NDWI to 92 % for EVI and SR. However, average intercept, slope, and  $R^2$  values were not significantly different among evaluation periods, except for  $R^2$  between the whole observation period and WW1 and between WW1 and WW2. Overall, EVI2 seemed to be the VI which explained most robustly the variability in observed daily NEE values across different crops

**Table 4.** Statistics of linear regression models of NEE and GPP versus VIs for 73 (whole observation period), 37 (both WW growing periods), 13 (first WW growing period – WW1), and 24 (second WW growing period – WW2) data pairs. All parameters were statistically significant at the level of  $p < 0.001$ , except where explicitly stated:  $p < 0.01$  (\*\*).

C flux	VI	Whole observation period			WW			WW1			WW2		
		Intercept	Slope	$R^2$	Intercept	Slope	$R^2$	Intercept	slope	$R^2$	Intercept	Slope	$R^2$
NEE*	EVI	1.87	1.29	0.84	1.91	1.36	0.88	1.82	1.44	0.92	1.91	1.4	<b>0.92</b>
	EVI2	1.85	1.49	<b>0.87</b>	1.89	1.56	<b>0.91</b>	1.78	1.64	<b>0.96</b>	1.86	1.71	0.86
	NDVI	1.67	1.4	0.86	1.56	1.63	0.88	1.56	1.61	0.9	1.52	1.72	0.82
	GNDVI	1.3	2.06	0.85	1.17	2.28	0.88	1.17	2.24	0.94	1.05	2.51	0.8
	SAVI	1.79	1.7	<b>0.87</b>	1.8	1.82	<b>0.91</b>	1.7	1.91	0.95	1.79	1.93	0.86
	NDWI	2.26	1.04	0.76	2.35	1.09	0.77	2.14	1.57	<b>0.96</b>	2.39	0.92	0.62
	S2REP	−33.61	0.05	0.76	−33.8	0.05	0.81	−37	0.05	0.92	−31.54	0.05	0.66
	SR	2.15	0.05	0.65	2.27	0.04	0.68	2.26	0.04	0.77	1.98	0.11	<b>0.92</b>
Mean	–	–	0.81	–	–	0.84	–	–	0.92	–	–	0.81	
GPP*	EVI	2.28	1.24	0.77	2.15	1.52	0.83	2.28	1.38	0.8	2.12	1.56	0.78
	EVI2	2.26	1.41	<b>0.78</b>	2.13	1.75	<b>0.84</b>	2.27	1.54	0.8	2.06	1.89	<b>0.81</b>
	NDVI	2.16	1.22	0.65	1.87	1.65	0.67	2.16	1.36**	0.61**	1.8	1.69	0.61
	GNDVI	1.83	1.8	0.64	1.45	2.34	0.69	1.79	1.95	0.68	1.34	2.46	0.6
	SAVI	2.21	1.6	0.77	2.04	2.01	0.82	2.21	1.76	0.77	1.98	2.12	0.8
	NDWI	2.63	1.04	0.76	2.63	1.3	0.81	2.59	1.48	0.82	2.63	1.14	0.74
	S2REP	−32.88	0.05	0.64	−38.1	0.06	0.77	−38	0.06	<b>0.94</b>	−32.47	0.05	0.54
	SR	2.53	0.05	0.61	2.56	0.04	0.62	2.71	0.03**	0.62**	2.22	0.12	0.76
Mean	–	–	0.7	–	–	0.76	–	–	0.76	–	–	0.71	

\* Note: NEE and GPP were both log-transformed; see text. To increase readability, the best-performing VIs (as indicated by  $R^2$ ) within a group are formatted in bold and worst-performing VIs within a group are formatted in italic.

and growing seasons; however, different VIs performed differently with varying crops or growing conditions.

For GPP, interception and slope parameters and the coefficient of determination were highly significant ( $p < 0.001$ ), except the slope and  $R^2$  of NDVI and SR in the WW1 growing period ( $p < 0.01$ ). Among evaluation periods, the mean values of interception, slope, and  $R^2$  were not significantly different. Linear regressions explained (significantly) less than for NEE, i.e., about 10 % ( $p < 0.05$ ) for the whole observation period, 8 % for the two WW growing periods, 16 % ( $p < 0.05$ ) for WW1, and 10 % for WW2. None of the mean values of the regression parameters were significantly different between NEE and GPP within one evaluation period. This suggested that GPP could be estimated with one generic regression model which is valid for different winter crops and different growing periods. However, this small dataset might not allow for this general conclusion.

As with NEE, EVI2 seemed to explain most of the variability in the GPP data for the whole observation period, the two WW growing periods, and the second WW growing period. S2REP showed the highest coefficient of determination for the WW1 period of 0.94, while it was rather low for the whole observation period, with a value of 0.64.

Juszczak et al. (2018) found an  $R^2$  value for the linear regression between ground-based and spectroscopy-based NDVI and SAVI, respectively, and GPP of WW of 0.56 and 0.59 ( $p < 0.0001$ ), respectively. Madugundu et al. (2017)

achieved  $R^2$  values of 0.81 ( $p = 0.04$ ), 0.86 ( $p = 0.02$ ), and 0.76 ( $p = 0.33$ ) for the linear regressions between GPP measurements during an irrigated maize-growing season and Landsat 8-derived NDVI, EVI, and LSWI, respectively. These values are based on only 11 d of measurements, which might be the reason for not showing high statistical significance. X. Huang et al. (2019) reported  $R^2$  values of 0.27 and 0.69 for NDVI and BRDF (bidirectional reflectance distribution function)-corrected NDVI, 0.83 and 0.03 for EVI and BRDF-corrected EVI, and 0.81 and 0.56 for EVI2 and BRDF-corrected EVI2 for the annual GPP of five cropland sites in the USA (rainfed maize) and Finland (spring barley on peat). When accounting for temperature, moisture stress, and photosynthetically active radiation, these values generally increased from between 0.4 and 0.6 to between 0.6 and 0.8 at the monthly scale. Overall, these results indicate a highly variable performance of linear regressions between VIs and cropland GPP, but EVI and EVI2 seem to outperform other VIs as proxies for GPP, as in our case and that of X. Huang et al. (2019).

Overall, our regressions for daily NEE and GPP showed a better fit to the C flux data than a similar study for grassland (Noumonvi et al., 2019). This might be attributable to the matched source area of EC and satellite data here; but more importantly, managed crops have a very distinct growing cycle which might also explain the better regression results. Still, our GPP regression model of NDVI and SAVI ex-

plained about 10 % more than the GPP regression models of Juszczak et al. (2018). The study by Madugundu et al. (2017) might not be considered robust enough for comparison of the hardly significant  $R^2$  values based on only 11 data pairs.

Further, our dataset allowed us to conclude that different crops could benefit from linear regression models based on different VIs for NEE, but this needs to be verified with more data.

### 3.5 Evaluation of estimated daily C fluxes

Continuous daily C fluxes were estimated by applying the linear regression models (Table 4) to daily interpolated VI values. The evaluation is discussed in terms of three aspects: (1) statistical measures of association and coincidence between estimates and measurements, for the different VIs, among observation periods, and between NEE and GPP; (2) comparing statistical measures for the temporal transferability (regressions of WW1 to estimate WW2 C fluxes); and (3) absolute errors in terms of the amount of seasonal accumulated C of NEE and GPP for WW2, from linear regressions based on WW1 to results from dedicated crop ecosystem models simulating WW and satellite data–model fusion approaches estimating cropland C fluxes.

#### 3.5.1 Association and coincidence

Overall, the order of statistical performance among VIs (Table 5) changed slightly compared with the evaluation of the linear regressions (Table 4).

Estimates of daily NEE values showed a better fit to the measured data than GPP estimates. However, only mean correlations ( $\rho$ ) and RMSEs were systematically statistically different between NEE and GPP when comparing within observation periods (Welch two-sample  $t$  test,  $R$ ). Individual statistical measures did not vary systematically, i.e., showing consistent improvements or downgrades, among evaluation periods (Table 5).

The mean coincidence of NEE estimates in terms of  $R^2$ , RMSE, and  $E$  improved from the whole observation period over WW to WW2; however, this improvement was only significant for mean  $R^2$  and RMSE values and only from the whole observation period to WW2. This supported the hypothesis that different VI models are needed to estimate C fluxes of individual crops. For the whole observation period, NEE was best estimated by EVI2, GNDVI, and SAVI with an average RMSE of  $2.13 \text{ g C m}^{-2} \text{ d}^{-1}$  and a modeling efficiency of 0.73. For the two WW growing periods, estimates with S2REP produced the lowest RMSE and the best modeling efficiency of  $1.72 \text{ g C m}^{-2} \text{ d}^{-1}$  and 0.81, respectively. The lowest performance was achieved with SR for all observation periods, except for  $R^2$  for WW2. For WW2, GNDVI gave the lowest RMSE of  $1.35 \text{ g C m}^{-2} \text{ d}^{-1}$ , the second-highest  $R^2$  value of 0.87, and a modeling efficiency of 0.86. Wohlfahrt et al. (2010) modeled daily NEE

values of two grassland sites for 1 and 2 years, respectively, using a light response model for GPP and a simple linear relationship between measured air temperature and measured Reco. The parameter estimates of maximum GPP and the apparent quantum yield of the light response model were based on the linear relationship to NDVI. This model explained 60 % and 80 % of measured daily NEE at two different grassland sites, respectively. However, NDVI values were derived from ground-based light sensors rather than satellites, thus exhibiting a different spatial resolution and representativeness than the satellite-derived VIs of our approach. Furthermore, the model was driven by half-hourly photosynthetically active radiation measurements, and NEE values were simulated for the same years which were used for their model parameterization. Still, despite using half-hourly radiation measurements to simulate daily NEE, the fraction of data variability explained was similar to or less than our results for NDVI.

Individual statistical evaluation measures for GPP estimates did not differ significantly among evaluation periods, except  $\rho$  and  $R^2$  between the whole observation period and WW2. Here, only  $R^2$  increased from the whole observation period to WW2, and as with NEE, the individual performance of VIs varied among evaluation periods. For the whole observation period, EVI, EVI2, and SAVI had a very similar performance for all statistical measures, and only the correlation ( $\rho$ ) of S2REP showed the highest values of 0.79 for this evaluation period.

#### 3.5.2 Evaluation of temporal transferability by comparing statistical measures

The mean coincidence of our NEE estimates for WW2 in terms of  $R^2$  and RMSE was 0.86 and  $1.64 \text{ g C m}^{-2} \text{ d}^{-1}$ , respectively (Table 5). These were very similar to simulation results from a dedicated crop model (SAFY-CO<sub>2</sub>) driven by satellite data for WW with  $R^2$  values of 0.78–0.9 and RMSE values of  $1.09$ – $1.59 \text{ g C m}^{-2} \text{ d}^{-1}$  (Pique et al., 2020). Pique et al. (2020) simulated 8 cropping years of WW at two agricultural sites in southwest France, with observed annual NEE values ranging from  $-208 \pm 19$  to  $-410 \pm 45 \text{ g C m}^2 \text{ yr}^{-1}$ . Arora (2003) simulated NEE of one WW growing season (doy 51–151) at an agricultural site in north-central Oklahoma (USA) using a coupled land surface terrestrial ecosystem model. RMSE values of  $2.37$  and  $2.69 \text{ g C m}^{-2} \text{ d}^{-1}$  and  $R^2$  values of 0.7 and 0.76 were achieved (Arora, 2003), which indicated a slightly lower accuracy than our approach. The ORCHIDEE-STICS (dynamic global vegetation model with the process-oriented crop model STICS) and the SPA (soil plant atmosphere) models showed lower mean  $R^2$  values of 0.75 and 0.83 and similar to higher RMSE values of between 1.2 and 3.1 and  $1.47 \text{ g C m}^{-2} \text{ d}^{-1}$ , respectively (Sus et al., 2010; Vuichard et al., 2016), compared with our values. ORCHIDEE-STICS and the SPA model were used to simulate seven WW growing seasons at seven agricultural

**Table 5.** Statistical evaluation of the final estimation of daily NEE and GPP from interpolated daily VI values for the whole observation period from the first to the last satellite image, i.e., 22 March 2020 to 16 August 2022, for the two WW growing periods (WW; from sowing to harvest) and the statistical evaluation of the estimation of the NEE and GPP fluxes for the second WW growing period (WW2) using the linear model from the first WW growing period (Table 4). All  $\rho$  and  $R^2$  values were statistically significant at the level of  $p < 0.001$  (\*\*\*). To increase readability, the best-performing VIs (as indicated by  $R^2$ ) within a group are formatted in bold and worst-performing VIs within a group are formatted in italic.

C flux	VI	Whole observation period				WW				WW2			
		$\rho$	$R^2$	RMSE	$E$	$\rho$	$R^2$	RMSE	$E$	$\rho$	$R^2$	RMSE	$E$
NEE	EVI	0.86	0.73	2.25	0.7	0.89	<b>0.89</b>	1.82	0.76	0.79	0.84	1.52	0.83
	EVI2	<b>0.87</b>	<b>0.75</b>	<b>2.15</b>	<b>0.73</b>	<b>0.9</b>	0.83	1.89	0.77	0.8	0.87	1.45	0.84
	NDVI	0.8	0.75	2.23	0.7	<b>0.9</b>	0.78	2.11	0.72	0.83	0.86	1.36	0.86
	GNDVI	<b>0.88</b>	<b>0.77</b>	<b>2.13</b>	<b>0.73</b>	<b>0.9</b>	0.8	1.98	0.75	<b>0.86</b>	<b>0.87</b>	<b>1.35</b>	<b>0.86</b>
	SAVI	<b>0.87</b>	<b>0.76</b>	<b>2.12</b>	<b>0.73</b>	<b>0.9</b>	0.83	1.88	0.78	0.81	0.88	1.38	0.86
	S2REP	0.84	0.74	2.39	0.66	0.86	0.82	<b>1.72</b>	<b>0.81</b>	0.88	0.82	1.73	0.77
	SR	0.87	0.53	3	<i>0.47</i>	<b>0.89</b>	0.59	2.75	<i>0.52</i>	0.81	0.89	2.72	<i>0.44</i>
	Mean	0.86	0.72	2.32	0.67	0.89	0.79	2.02	0.73	0.83	0.86	1.64	0.78
GPP	EVI	0.76	0.76	3.32	0.71	0.74	0.8	3.24	0.74	0.68	0.85	2.8	0.72
	EVI2	<b>0.76</b>	<b>0.76</b>	<b>3.26</b>	<b>0.72</b>	0.73	0.8	3.25	0.74	0.69	<b>0.88</b>	<b>2.6</b>	<b>0.75</b>
	NDVI	0.68	0.63	4.1	0.57	0.66	0.65	4.05	0.6	0.67	0.77	4.17	0.38
	GNDVI	0.7	0.64	3.96	0.58	0.69	0.69	3.75	0.66	0.7	0.78	3.73	0.5
	SAVI	0.75	0.75	3.34	0.71	0.73	0.78	3.32	0.73	0.69	0.87	2.75	0.73
	S2REP	<b>0.79</b>	0.73	3.33	0.71	<b>0.83</b>	<b>0.85</b>	<b>2.48</b>	<b>0.85</b>	<b>0.74</b>	0.81	2.72	0.74
	SR	0.69	0.53	4.53	<i>0.46</i>	0.69	0.55	4.64	<i>0.47</i>	0.65	0.84	5.05	<i>0.09</i>
	Mean	0.73	0.69	3.69	0.64	0.72	0.73	3.53	0.68	0.69	0.83	3.4	0.56

sites and eight WW growing seasons at six agricultural sites in central Europe, respectively (Sus et al., 2010; Vuichard et al., 2016). The simulations were carried out at mostly the same European sites where observed NEE values ranged from  $-529$  to  $-169$   $\text{g C m}^{-2}$  (Sus et al., 2010) and from  $-451$  to  $15$   $\text{g C m}^{-2}$  (Vuichard et al., 2016).

A comprehensive crop model inter-comparison study, carried out at the aforementioned European cropland sites, however, showed a very high variability in model performances simulating C fluxes of WW. The  $\tau$  values (Kendall correlation coefficient; as used in Wattenbach et al., 2010) ranged from 0.28 to 0.81 (mean = 0.58) for growing season NEE and modeling efficiency ( $E$ ) values spread between 0.31 and 0.87 (mean = 0.55) (Wattenbach et al., 2010), while our respective mean  $E$  values ranged from 0.44 to 0.86. Our GPP estimates showed lower accuracy than the modeling exercise that was previously mentioned in which  $R^2$  and RMSE values were 0.86–0.96 and 0.9–2.79  $\text{g C m}^{-2} \text{d}^{-1}$  for GPP (Pique et al., 2020) as compared with our mean values of 0.83 and 3.4  $\text{g C m}^{-2} \text{d}^{-1}$  for WW2, respectively. GPP was simulated similarly well with the models in Wattenbach et al. (2010) compared to our approach. Our mean  $\rho$  for GPP estimates for WW2 was 0.69, and the mean  $E$  was 0.56; the respective mean values from Wattenbach et al. (2010) were 0.58 for  $\tau$  and 0.65 for  $E$ . ORCHIDEE-STICS showed  $R$  values over 0.7 for the growing season GPP of WW (Vuichard et al., 2016).

The differences between observed and estimated NEE and GPP in this study are visually exemplified for EVI2 in Fig. 5.

We also put our results into perspective with a number of studies which use high-resolution satellite-based VIs in combination with mechanistic or machine learning approaches to estimate daily C fluxes for croplands. Fu et al. (2014) diagnosed cropland NEE using a regression tree model in combination with highly processed Landsat imagery and NDVI and EVI. At the four cropland sites (rainfed maize, USA) in their study, they achieved  $R^2$  and RMSE values of 0.66–0.91 and 1.95–2.34  $\text{g C m}^{-2} \text{d}^{-1}$ , respectively, where observed and diagnosed NEE were  $-0.68$  (0.24 standard deviation) and  $-1.4$  (0.28 standard deviation)  $\text{g C m}^{-2} \text{d}^{-1}$ , respectively. They speculated that the overestimation of C uptake is due to the “ill parameterization” of their statistical model because of the low number of cropland sites. They do not leverage the information about the different site characteristics to further explore the large variability in the model performance between the different sites. Bazzi et al. (2024) evaluated the performance of a modified vegetation–photosynthesis–respiration model supported by Sentinel-2 LSWI and EVI, simulating NEE, GPP, and Reco at 12 European cropland sites (range of crops including WW) for the period 2018–2020. The  $R^2$  values ranged from 0.72 to 0.86 for daily NEE, 0.81 to 0.86 for daily GPP, and 0.38 to 0.77 for daily Reco. It should be noted, however, that this accuracy measure was not a cross-validation result but was for the same



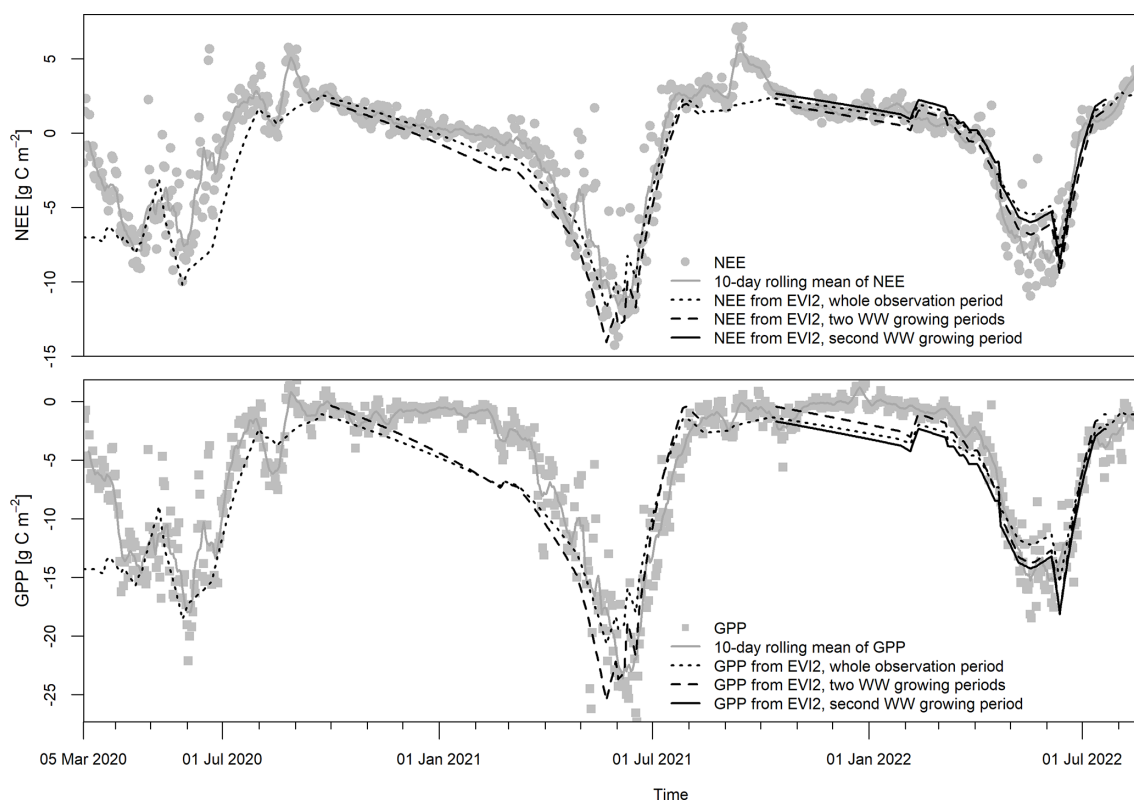


**Figure 5.** Measured (gray points and lines) and estimated daily NEE and GPP for the whole period (dotted black) for the two WW growing periods (dashed black) and for the second WW growing period (solid black). Estimated NEE and GPP values for the whole period were imputed from the linear regression from the whole observation period, NEE and GPP values for the two WW growing periods were calculated from the linear regression based on the two WW growing periods, and NEE and GPP of the second WW growing period were based on the linear regression from the first WW growing season only.

site years as used for parameter optimization. A combination of mechanistic modeling, Sentinel-2 or Landsat 8 optical remote sensing data, and machine learning algorithms was actually needed to achieve  $R^2$  values of 0.91 and 0.82 with Sentinel-2 and Landsat 8 data, respectively, for daily GPP estimates for 6 cropland site years (soybean, winter wheat, winter barley, clover) (Wolanin et al., 2019).

While all these approaches do generally show a similar or higher accuracy compared with our approach, a much higher effort is needed to derive NEE and GPP estimates.

### 3.5.3 Absolute errors of temporal transferability

Absolute deviations between the measured seasonal C fluxes of NEE and GPP and our estimates for every VI are displayed in Table 6. Total NEE estimates ranged from an underestimation of C uptake of  $195.8 \text{ g C m}^{-2}$  (85.66 %, S2REP) to an overestimation of  $57.24 \text{ g C m}^{-2}$  (25.04 %, SR) (Table 6). The best estimates were achieved with NDVI and GNDVI, with an overestimation of C uptake of  $33.36 \text{ g C m}^{-2}$  (14.59 %) and an underestimation of  $40.98 \text{ g C m}^{-2}$  (17.93 %), respectively. Both VIs had the low-

est RMSE values of 1.36 and  $1.35 \text{ g C m}^{-2}$ , respectively, when estimating daily C fluxes (Table 5).

The model ensemble of Wattenbach et al. (2010) exhibited simulation errors of total annual C sums ranging from an overestimation from the measured C uptake of  $204 \text{ g C m}^{-2}$  to an underestimation of C uptake of  $217 \text{ g C m}^{-2}$  across the 5 WW site years and three crop models used in their study. The simulated seasonal C uptake (NEE) by ORCHIDEE-STICS ranged from an overestimation of C uptake of  $251 \text{ g C m}^{-2}$  (1673 %) to an underestimation of C uptake of  $321 \text{ g C m}^{-2}$  (108 %) (Vuichard et al., 2016). The SPA model had a tendency to overestimate C uptake (NEE) ranging from 5 (0.9 %) to  $289 \text{ g C m}^{-2}$  (92 %) for 8 WW site years in Europe (Sus et al., 2010). This comparison highlights again that sophisticated mechanistic ecosystem models are not a priori superior to simple regression approaches.

Discrepancies in our best NEE estimations were in the same range as our estimated uncertainty of 0.8 and  $13 \text{ g C m}^{-2}$  for 2020–2021 and 2021–2022, respectively, and reported NEE uncertainties of  $40 \text{ g C m}^{-2}$  of WW crops (Aubinet et al., 2009; Béziat et al., 2009). Further, estimation uncertainty is smaller than the difference of the total growing

**Table 6.** Differences in observed and estimated cumulated C fluxes for the second WW growing period (WW2) using WW1-based regression models. For the interpretation of NEE results, negative absolute values and positive percent values denote an underestimation of C uptake compared with the observed C uptake. For the interpretation of GPP results, negative absolute values and negative percent values denote an overestimation of C uptake compared with the observed C uptake. Note that numbers in bold indicate regression models which produce the lowest error for estimating NEE and GPP.

C flux (measured)	VI	Estimates ( $\text{g C m}^{-2}$ )	Total difference ( $\text{g C m}^{-2}$ )	Difference (%)
WW2				
NEE −228.58	EVI	−117.00	−111.58	48.81
	EVI2	−62.48	−166.10	72.67
	NDVI	−261.93	<b>33.36</b>	<b>−14.59</b>
	GNDVI	−187.60	<b>−40.98</b>	<b>17.93</b>
	SAVI	−86.38	−142.19	62.21
	S2REP	−32.78	−195.80	85.66
	SR	−285.81	57.24	−25.04
	Mean		−147.71	−80.86
GPP 1165	EVI	1712.15	−547.18	−46.97
	EVI2	1663.08	−498.12	−42.76
	NDVI	2090.09	−925.12	−79.41
	GNDVI	1945.69	−780.73	−67.02
	SAVI	1723.97	−559.01	−47.98
	S2REP	1458.13	<b>−293.17</b>	<b>−25.17</b>
	SR	2018.80	−853.84	−73.29
	Mean		1801.7	−636.74

season NEE between the two WW growing periods 2020–2021 and 2021–2022, respectively, which was  $311 \text{ g C m}^{-2}$  (i.e.,  $3.11 \text{ t C ha}^{-1}$ , Table 3).

Larger differences occurred between the measured and estimated GPP fluxes. Estimated GPP overestimated absolute measured flux values from 25 % up to 79 %. The latter was due to the overestimation of C uptake during winter (as exemplified in Fig. 5) when VI values indicated a vital crop growth inferred from relatively high crop greenness values as explained earlier (see Sect. 3.2). Here, the previously mentioned issue of diverting NEE and VI signals after sowing and during winter (Sect. 3.2) showed its effect, causing a larger discrepancy between observed and estimated GPP for the WW growing period. Deviations of our estimated GPP values were higher than simulated GPP values of the mechanistic crop model ORCHIDEE-STICS, ranging from an underestimation of 42 % to an overestimation of 20 % for the WW growing seasons (Vuichard et al., 2016).

A variety of explanations are discussed for the ecosystem models failing to simulate C exchange over growing seasons. Models face problems in representing phases of low C fluxes (such as winter) (Dietiker et al., 2010; Wattenbach et al., 2010), or the models assume post-harvest phases to be bare soil, ignoring regrowth from weeds and/or leftover seeds and thus underestimating C uptake (Lu et al., 2017; Vuichard et al., 2016). The importance of capturing spontaneous regrowth, which can usually not be simulated by mechanistic crop growth models unless specifically param-

eterized for, has been pointed out in relation to the advantages of using remote sensing data in crop modeling. Especially the knowledge of key dates, such as time of emergence, maximum vegetation, start of senescence, and harvest, determines the accuracy of model estimations (Pique et al., 2020). While our approach struggled with the low-flux time during winter as well, the high resolution of Sentinel-2 imagery, especially during non-winter seasons, is well suited to pick up the plant growth dynamics on the respective key dates without knowing them explicitly. In conjunction with the good performance of our estimates using linear regression only, our approach constitutes a promising alternative of very low data demand to estimate C exchange of a highly dynamic and heterogeneous small-parceled landscape.

Vuichard et al. (2016) and Sus et al. (2010) further discussed issues related to the representation of phenology in the models, which is a determining factor for the subsequent calculation of C fluxes. Now, using the actual spectral optical properties of crops directly – as in our approach – might constitute an advantage in tracking the actual phenology and thus the associated evolution of C fluxes.

### 3.6 Strengths and weaknesses of the approach

Finally, the strengths and weaknesses of the approach are briefly discussed. Weaknesses were the use of simple linear regression models, which are empirical and not mechanistic-

cal, and considerable evaluation and proof of concept are still needed before the approach can be applied spatially.

As explained in the Introduction, NEE is only indirectly linked to spectral VIs via the direct correlation of GPP with spectral VIs and the observed correlation between GPP and Reco. Since the sum of negative GPP and positive Reco gives NEE, the direct link of NEE to spectral VI was justified. In our study, GPP and Reco were significantly ( $p < 0.001$ ) correlated by  $-0.63$  (Spearman's correlation), but GPP and NEE had an even better correlation by  $0.95$  ( $p < 0.001$ ; using cases with NEE qc = 0 measurements only). Furthermore, correlations between NEE and VIs were stronger than correlations between GPP and VIs (Fig. 4). Considering these highly significant and strong correlations, a direct empirical and linear link between GPP and VIs and even more between NEE and VIs seemed justified and sufficiently proven.

However, the high correlation between NEE and VI hides the problematic diversion of signals during winter. Here, the very few VI images during winter showed a better correlation than might have been observed with more winter VI data. Thus, the decoupling of the signals needs to be further addressed. Theoretically, the lowest VI values should be linked with bare soil or very little vegetation and thus mainly Reco. This assumption is invalidated by the winter increase in VI values. If this non-active-growing period were treated differently than the spring–summer period, it could be cut out from the correlations and would need to be replaced by another assumption, such as assuming a baseline winter C flux. The associated questions would be how variable baseline respiration at croplands is, what the proportion of winter fluxes to the total is, and what impact that would have on the total results if it varies.

The most prominent question which now remains is whether the linear regressions fitted here hold for crops other than winter grains, such as maize or root crops, or are they grain-crop-type specific? Juszczak et al. (2018) argue that a generic single relationship between VI and C flux can be valid for a range of different crops.

The strengths of this approach are the low data demand, the straightforwardness, and the accuracy compared with ecosystem models and satellite data–model fusion approaches, which are the most sophisticated approaches for estimating spatial C exchange, and, by monitoring plant “greenness” directly, the highly complex plant growth is integrated into a representative signal.

#### 4 Conclusions and outlook

The observed CO<sub>2</sub> dynamics of the cropland site presented here were representative of a typical winter rape and winter wheat cropland in Europe. The site was thus suitable for developing a generic approach of linking remote sensing data with EC measurements. A linking approach consisting of multiple evaluation steps was developed by appropriately

accounting for spatial alignments between EC measurement footprints and remote sensing data of fine spatial resolutions. This rigorous linking approach was applied to a range of VIs to evaluate their strengths and weaknesses in estimating daily CO<sub>2</sub> fluxes for the search of the most promising VIs. The general validity of the approach was shown by the high and statistically significant linear correlations between C fluxes and VIs. However, the ranking of the suitability of VIs differed among the evaluation by the linear correlation, the linear regression, and the temporal transferability, indicating no single stable or universally superior VI for daily CO<sub>2</sub> flux estimation. While linear regressions suggested S2REP as the most promising VI for estimating WW NEE, NDVI and GNDVI were the best for the temporal transferability of WW NEE estimations. Overall, the approach leads to results similar to those of complex ecosystem models or sophisticated satellite data–model fusion approaches, which justifies the data-driven and data-lean approach. Relatively small estimation errors at this stage of research further suggest that this approach is a promising method for tracking C exchange remotely over croplands. Future work should mainly address three questions: does one generic relationship between VIs and C fluxes hold for other crop types and/or climate conditions as well? Which VIs are most suitable for estimating which C flux? And, does any additional information, such as temperature or radiation for light use efficiency modeling, further improve accuracy? Or from a more overarching perspective, which processes or data uncertainties explain the gap between measured and estimated C fluxes?

#### Appendix A: EC data quality control

To assure a robust time series of half-hourly flux measurements, “qc0 data” were further screened for outliers by calculating half-hourly median and standard deviations of a 30 d moving window and testing each half-hour flux measurement against the respective half-hour statistics. Fluxes exceeding the median  $\pm 2$  (daytime) and  $\pm 3$  (nighttime) standard deviations were excluded from the time series (similarly to Goodrich et al., 2015). This was followed by a visual inspection of plotting diurnal half-hourly fluxes against monthly diurnal means. This yielded some extreme values which were within the previously defined bounds but which still strongly biased the median and standard calculation in the previous step in times of high occurrence of gaps. These values were removed, and the 30 d moving window statistics loop was iterated.

#### Appendix B: Filtering fluxes of main field with FP modeling

Figure 1 (in the main text) shows the cumulative source area of the EC measurements extending over adjacent fields. To construct a spatially representative NEE time series of

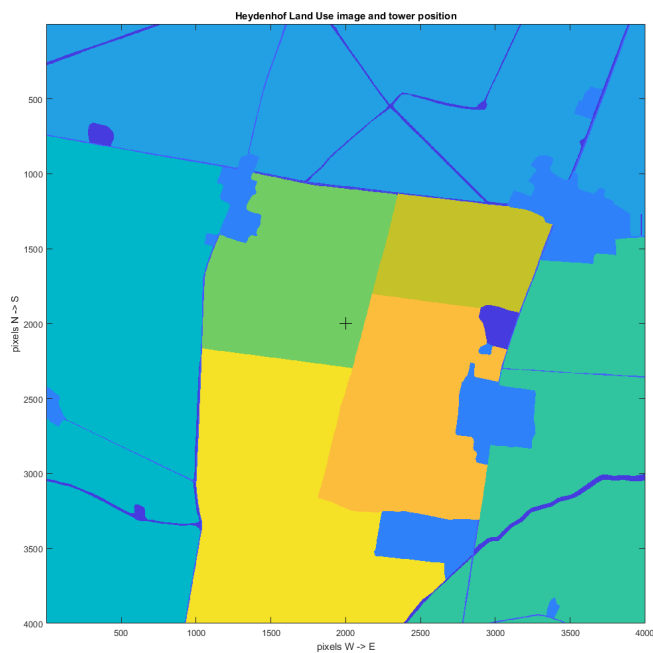


**Figure B1.** Land use image of Heydenhof used for applying the analytical FP model. Different colors distinguish the different fields and land use types used to determine source area contributions. The + indicates the location of the EC tower. The green field in the middle where the + symbol is located is the main field.

the main field excluding surrounding areas, measured fluxes were combined with FP modeling following the approach of Göckede et al. (2004). The source area of the flux measurements is heterogeneous in space (Fig. 1) and time, and its distribution varies with changing meteorological conditions. Stable atmospheric conditions enlarge the FP, usually during the nighttime, while unstable conditions during the daytime decrease the size of the FP. Thus, each flux measurement carries a mixed signal of fluxes originating to a variable degree from different surface areas. To quantify the contribution of different surface areas to the total half-hourly flux, analytical FP models are employed (Göckede et al., 2004). Here the analytical FP model by Kormann and Meixner (2001) was used. The land use map was constructed by classifying visible homogeneous land use areas from a Google Earth image (same as in Fig. 1 of the main text) in the form of a discrete matrix (Fig. B1).

Gaps in wind direction measurements caused respective gaps in the FP results. The 0.6 % missing wind direction measurements, with the longest gap of 9 h, were filled by linear interpolation. In turn, the gaps in the FP results were filled by assigning the gaps the average values of FP results of respective  $1^\circ$  wind direction bins.

According to Göckede et al. (2008), fluxes with a 95 % contribution of a specified source area to the total flux are termed “homogeneous measurements”, while fluxes with an 80 %–95 % contribution are still regarded as “representative

measurements”. However, these limits were set based on intensive pre-analyses and practicability.

### Appendix C: Gap filling and partitioning of flux data

For calculating C budgets from NEE data, a continuous time series is required. To avoid periods of insufficient turbulence which violate EC assumptions and could bias nighttime fluxes, i.e., ecosystem respiration, data were filtered by a  $u^*$  threshold that determines low-turbulence conditions. Here, the  $u^*$  threshold was calculated by the moving point method (Papale et al., 2006). Subsequently, the NEE time series was gap-filled by the marginal distribution sampling (MDS) approach of Reichstein et al. (2005), which has been widely used for arable EC flux measurements (Béziat et al., 2009; Pastorello et al., 2020).

The  $u^*$  estimation, gap-filling, uncertainty estimation by bootstrapping, and flux partitioning were carried out with the R package “REddyProc” (Wutzler et al., 2018) available from <https://cran.r-project.org/web/packages/REddyProc/index.html> (last access: 12 August 2024).

### Appendix D

A comprehensive cropland soil C budget encompasses a number of C flows in addition to GPP, Reco, manure and seed inputs, and harvest exports. These include C losses due to fire, wind, and water erosion; leaching of dissolved organic C (DOC) and volatile organic compound (VOC) losses (Ciais et al., 2010); exchange in the form of CO and CH<sub>4</sub>; and C input from deposition (Waldo et al., 2016). Losses due to fire can be ignored for our field. Erosion and deposition can be assumed to be canceled out due to the surrounding area being of the same nature as our main field. CO, CH<sub>4</sub>, and VOC can be considered negligible for a regular cropping field (Waldo et al., 2016) as can leaching losses of DOC (Siemens et al., 2012).

*Code availability.* The MATLAB, R, and JavaScript codes for flux and satellite data processing including quality control, analyses, and visualization as produced for this paper are available via <https://doi.org/10.5880/GFZ.1.4.2024.002> (Gottschalk et al., 2024a).

*Data availability.* Half-hourly flux data and auxiliary meteorological data for this article in standard EddyPro output, a shape file outlining the main field borders, and the TERENO precipitation data are available via <https://doi.org/10.5880/GFZ.1.4.2024.001> (Gottschalk et al., 2024b). Continuous half-hourly eddy covariance and micrometeorological data are available on request via the European Fluxes Database Cluster (<http://www.europe-fluxdata.eu/home/site-details?id=DE-Hdn>, last access: 13 August 2024).

*Supplement.* The supplement related to this article is available online at: <https://doi.org/10.5194/bg-21-3593-2024-supplement>.

*Author contributions.* PG: conceptualization, methodology, software, formal analyses, validation, visualization, writing – original draft and review and editing. AK: writing – review and editing. CW: data curation, software, writing – review and editing. ZL: software, writing – review and editing. TS: resources, writing – review and editing, supervision, project administration, funding acquisition. All authors have read and agreed to the published version of the paper.

*Competing interests.* The contact author has declared that none of the authors has any competing interests.

*Disclaimer.* Publisher's note: Copernicus Publications remains neutral with regard to jurisdictional claims made in the text, published maps, institutional affiliations, or any other geographical representation in this paper. While Copernicus Publications makes every effort to include appropriate place names, the final responsibility lies with the authors.

*Acknowledgements.* We thank Karl Kemper (GFZ intern) for preparing the land use matrix for the footprint modeling and providing Figs. 1 and B1. We further acknowledge Youping Li, who developed the first draft of the GEE (Google Earth Engine) scripts during a scientific visit at GFZ.

*Financial support.* This research has been supported by the German Federal Ministry of Food and Agriculture (BMEL) in the frame of the ERA-NET FACCE ERA-GAS project GHG-manage, grant no. 2817ERA10C. FACCE ERA-GAS has received funding from the European Union's Horizon 2020 research and innovation program under grant agreement no. 696356. We further used infrastructure of the Terrestrial Environmental Observatories Network (TERENO).

The article processing charges for this open-access publication were covered by the Helmholtz Centre Potsdam–GFZ German Research Centre for Geosciences.

*Review statement.* This paper was edited by Andrew Feldman and reviewed by two anonymous referees.

## References

Anthoni, P. M., Freibauer, A., Kolle, O., and Schulze, E.-D.: Winter wheat carbon exchange in Thuringia, Germany, *Agr. Forest Meteorol.*, 121, 55–67, [https://doi.org/10.1016/S0168-1923\(03\)00162-X](https://doi.org/10.1016/S0168-1923(03)00162-X), 2004.

Arora, V. K.: Simulating energy and carbon fluxes over winter wheat using coupled land surface and terrestrial

ecosystem models, *Agr. Forest Meteorol.*, 118, 21–47, [https://doi.org/10.1016/S0168-1923\(03\)00073-X](https://doi.org/10.1016/S0168-1923(03)00073-X), 2003.

Aubinet, M., Moureaux, C., Bodson, B., Dufranne, D., Heinesch, B., Suleau, M., Vancutsem, F., and Vilret, A.: Carbon sequestration by a crop over a 4-year sugar beet/winter wheat/seed potato/winter wheat rotation cycle, *Agr. Forest Meteorol.*, 149, 407–418, <https://doi.org/10.1016/j.agrformet.2008.09.003>, 2009.

Badgley, G., Field, C. B., and Berry, J. A.: Canopy near-infrared reflectance and terrestrial photosynthesis, *Sci. Adv.*, 3, e1602244, <https://doi.org/10.1126/sciadv.1602244>, 2017.

Baldocchi, D.: Breathing of the terrestrial biosphere: lessons learned from a global network of carbon dioxide flux measurement systems, *Aust. J. Bot.*, 56, 1–26, <https://doi.org/10.1071/BT07151>, 2008.

Baldocchi, D., Sturtevant, C., and Contributors, F.: Does day and night sampling reduce spurious correlation between canopy photosynthesis and ecosystem respiration?, *Agr. Forest Meteorol.*, 207, 117–126, <https://doi.org/10.1016/j.agrformet.2015.03.010>, 2015.

Baldocchi, D. D.: Assessing the eddy covariance technique for evaluating carbon dioxide exchange rates of ecosystems: past, present and future, *Glob. Change Biol.*, 9, 479–492, <https://doi.org/10.1046/j.1365-2486.2003.00629.x>, 2003.

Bazzi, H., Ciais, P., Abbessi, E., Makowski, D., Santaren, D., Ceschia, E., Brut, A., Tallec, T., Buchmann, N., Maier, R., Acosta, M., Loubet, B., Buysse, P., Léonard, J., Bornet, F., Fayad, I., Lian, J., Baghdadi, N., Segura Barrero, R., Brümmel, C., Schmidt, M., Heinesch, B., Mauder, M., and Gruenwald, T.: Assimilating Sentinel-2 data in a modified vegetation photosynthesis and respiration model (VPRM) to improve the simulation of croplands CO<sub>2</sub> fluxes in Europe, *Int. J. Appl. Earth Obs.*, 127, 103666, <https://doi.org/10.1016/j.jag.2024.103666>, 2024.

Béziat, P., Ceschia, E., and Dedieu, G.: Carbon balance of a three crop succession over two cropland sites in South West France, *Agr. Forest Meteorol.*, 149, 1628–1645, <https://doi.org/10.1016/j.agrformet.2009.05.004>, 2009.

Boegh, E., Soegaard, H., Broge, N., Hasager, C. B., Jensen, N. O., Schelde, K., and Thomsen, A.: Airborne multispectral data for quantifying leaf area index, nitrogen concentration, and photosynthetic efficiency in agriculture, *Remote Sens. Environ.*, 81, 179–193, [https://doi.org/10.1016/S0034-4257\(01\)00342-X](https://doi.org/10.1016/S0034-4257(01)00342-X), 2002.

Chandrasekar, K., Sessa Sai, M. V. R., Roy, P. S., and Dwevedi, R. S.: Land Surface Water Index (LSWI) response to rainfall and NDVI using the MODIS Vegetation Index product, *Int. J. Remote Sens.*, 31, 3987–4005, <https://doi.org/10.1080/01431160802575653>, 2010.

Chapin, F. S., Woodwell, G. M., Randerson, J. T., Rastetter, E. B., Lovett, G. M., Baldocchi, D. D., Clark, D. A., Harmon, M. E., Schimel, D. S., Valentini, R., Wirth, C., Aber, J. D., Cole, J. J., Goulden, M. L., Harden, J. W., Heimann, M., Howarth, R. W., Matson, P. A., McGuire, A. D., Melillo, J. M., Mooney, H. A., Neff, J. C., Houghton, R. A., Pace, M. L., Ryan, M. G., Running, S. W., Sala, O. E., Schlesinger, W. H., and Schulze, E. D.: Reconciling Carbon-cycle Concepts, Terminology, and Methods, *Ecosystems*, 9, 1041–1050, <https://doi.org/10.1007/s10021-005-0105-7>, 2006.

Chen, B., Ge, Q., Fu, D., Yu, G., Sun, X., Wang, S., and Wang, H.: A data-model fusion approach for upscaling gross ecosys-

- tem productivity to the landscape scale based on remote sensing and flux footprint modelling, *Biogeosciences*, 7, 2943–2958, <https://doi.org/10.5194/bg-7-2943-2010>, 2010.
- Ciais, P., Wattenbach, M., Vuichard, N., Smith, P., Piao, S. L., Don, A., Luysaert, S., Janssens, I. A., Bondeau, A., Dechow, R., Leip, A., Smith, P., Beer, C., Van der Werf, G. R., Gervois, S., Van Oost, K., Tomelleri, E., Freibauer, A., Schulze, E. D., and CARBOEUROPE Synthesis Team: The European carbon balance. Part 2: croplands, *Glob. Change Biol.*, 16, 1409–1428, <https://doi.org/10.1111/j.1365-2486.2009.02055.x>, 2010.
- Dietiker, D., Buchmann, N., and Eugster, W.: Testing the ability of the DNDC model to predict CO<sub>2</sub> and water vapour fluxes of a Swiss cropland site, *Agr. Ecosyst. Environ.*, 139, 396–401, <https://doi.org/10.1016/j.agee.2010.09.002>, 2010.
- Frampton, W. J., Dash, J., Watmough, G., and Milton, E. J.: Evaluating the capabilities of Sentinel-2 for quantitative estimation of biophysical variables in vegetation, *ISPRS J. Photogramm.*, 82, 83–92, <https://doi.org/10.1016/j.isprsjprs.2013.04.007>, 2013.
- Fu, D., Chen, B., Zhang, H., Wang, J., Black, T. A., Amiro, B. D., Bohrer, G., Bolstad, P., Coulter, R., Rahman, A. F., Dunn, A., McCaughey, J. H., Meyers, T., and Verma, S.: Estimating landscape net ecosystem exchange at high spatial–temporal resolution based on Landsat data, an improved upscaling model framework, and eddy covariance flux measurements, *Remote Sens. Environ.*, 141, 90–104, <https://doi.org/10.1016/j.rse.2013.10.029>, 2014.
- Gao, B.-C.: NDWI—A normalized difference water index for remote sensing of vegetation liquid water from space, *Remote Sens. Environ.*, 58, 257–266, [https://doi.org/10.1016/S0034-4257\(96\)00067-3](https://doi.org/10.1016/S0034-4257(96)00067-3), 1996.
- Gitelson, A. A., Kaufman, Y. J., and Merzlyak, M. N.: Use of a green channel in remote sensing of global vegetation from EOS-MODIS, *Remote Sens. Environ.*, 58, 289–298, [https://doi.org/10.1016/S0034-4257\(96\)00072-7](https://doi.org/10.1016/S0034-4257(96)00072-7), 1996.
- Gitelson, A. A., Peng, Y., Masek, J. G., Rundquist, D. C., Verma, S., Suyker, A., Baker, J. M., Hatfield, J. L., and Meyers, T.: Remote estimation of crop gross primary production with Landsat data, *Remote Sens. Environ.*, 121, 404–414, <https://doi.org/10.1016/j.rse.2012.02.017>, 2012.
- Göckede, M., Rebmann, C., and Foken, T.: A combination of quality assessment tools for eddy covariance measurements with footprint modelling for the characterisation of complex sites, *Agr. Forest Meteorol.*, 127, 175–188, <https://doi.org/10.1016/j.agrformet.2004.07.012>, 2004.
- Göckede, M., Foken, T., Aubinet, M., Aurela, M., Banza, J., Bernhofer, C., Bonnefond, J. M., Brunet, Y., Carrara, A., Clement, R., Dellwik, E., Elbers, J., Eugster, W., Fuhrer, J., Granier, A., Grünwald, T., Heinesch, B., Janssens, I. A., Knohl, A., Koebler, R., Laurila, T., Longdoz, B., Manca, G., Marek, M., Markkanen, T., Mateus, J., Matteucci, G., Mauder, M., Migliavacca, M., Minerbi, S., Moncrieff, J., Montagnani, L., Moors, E., Ourcival, J.-M., Papale, D., Pereira, J., Pilegaard, K., Pita, G., Rambal, S., Rebmann, C., Rodrigues, A., Rotenberg, E., Sanz, M. J., Sedlak, P., Seufert, G., Siebicke, L., Soussana, J. F., Valentini, R., Vesala, T., Verbeeck, H., and Yakir, D.: Quality control of CarboEurope flux data – Part 1: Coupling footprint analyses with flux data quality assessment to evaluate sites in forest ecosystems, *Biogeosciences*, 5, 433–450, <https://doi.org/10.5194/bg-5-433-2008>, 2008.
- Goodrich, J. P., Campbell, D. I., Clearwater, M. J., Rutledge, S., and Schipper, L. A.: High vapor pressure deficit constrains GPP and the light response of NEE at a Southern Hemisphere bog, *Agr. Forest Meteorol.*, 203, 54–63, <https://doi.org/10.1016/j.agrformet.2015.01.001>, 2015.
- Gorelick, N., Hancher, M., Dixon, M., Ilyushchenko, S., Thau, D., and Moore, R.: Google Earth Engine: Planetary-scale geospatial analysis for everyone, *Remote Sens. Environ.*, 202, 18–27, <https://doi.org/10.1016/j.rse.2017.06.031>, 2017.
- Gottschalk, P., Kalhori, A., Li, Z., Wille, C., and Sachs, T.: Code for linking half-hourly CO<sub>2</sub> eddy covariance flux data with Sentinel-2 derived vegetation indices (7) for 05/03/2020 – 23/08/2022, GFZ Data Service [code], <https://doi.org/10.5880/GFZ.1.4.2024.002>, 2024a.
- Gottschalk, P., Kalhori, A., Li, Z., Wille, C., and Sachs, T.: Half-hourly CO<sub>2</sub> eddy covariance flux data, associated meteorological data and Sentinel-2 derived vegetation indices (7) for 05/03/2020 – 23/08/2022, GFZ Data Service [data set], <https://doi.org/10.5880/GFZ.1.4.2024.001>, 2024b.
- Grace, J., Nichol, C., Disney, M., Lewis, P., Quaife, T., and Bowyer, P.: Can we measure terrestrial photosynthesis from space directly, using spectral reflectance and fluorescence?, *Glob. Change Biol.*, 13, 1484–1497, <https://doi.org/10.1111/j.1365-2486.2007.01352.x>, 2007.
- Guo, L. B. and Gifford, R. M.: Soil carbon stocks and land use change: a meta analysis, *Glob. Change Biol.*, 8, 345–360, <https://doi.org/10.1046/j.1354-1013.2002.00486.x>, 2002.
- Guyot, G. and Baret, F.: Utilisation de la haute resolution spectrale pour suivre l'état des couverts vegetaux, 4th International Colloquium “Spectral Signatures of Objects in Remote Sensing”, 1988ESASP.287..279G, Aussois, 18–22 January, 279–286, 1988.
- Huang, C. J., Qiao, F., Chen, S., Xue, Y., and Guo, J.: Observation and Parameterization of Broadband Sea Surface Albedo, *J. Geophys. Res.-Oceans*, 124, 4480–4491, <https://doi.org/10.1029/2018JC014444>, 2019.
- Huang, X., Xiao, J., and Ma, M.: Evaluating the Performance of Satellite-Derived Vegetation Indices for Estimating Gross Primary Productivity Using FLUXNET Observations across the Globe, *Remote Sens.*, 11, 1823, <https://doi.org/10.3390/rs11151823>, 2019.
- Huete, A. R.: A soil-adjusted vegetation index (SAVI), *Remote Sens. Environ.*, 25, 295–309, [https://doi.org/10.1016/0034-4257\(88\)90106-X](https://doi.org/10.1016/0034-4257(88)90106-X), 1988.
- Itzerott, S. and Kaden, K.: Ein neuer Algorithmus zur Klassifizierung landwirtschaftlicher Fruchtarten auf Basis spektraler Normkurven, *Photogramm. Fernerkun.*, 6, 509–518, 2006a.
- Itzerott, S. and Kaden, K.: Spektrale Normkurven - eine notwendige Voraussetzung für die Klassifizierung der Fruchtartenverteilung aus Fernerkundungsdaten, *Photogramm. Fernerkun.*, 3, 205–216, 2006b.
- Itzerott, S., Hohmann, C., Künzel, A., Budach, C., Stender, V., Brinckmann, N., Maass, H., Borg, E., Renke, F., Jahnncke, D., Berg, M., Schmidt, K., Wegener, M., Conrad, C., and Spengler, D.: TERENO (Northeast), Climate station Heydenhof, Germany, V. 2.5., GFZ Data Services [data set], <https://doi.org/10.5880/TERENO.GFZ.2018.024>, 2018.
- Jiang, Z., Huete, A. R., Didan, K., and Miura, T.: Development of a two-band enhanced vegetation index with-



- out a blue band, *Remote Sens. Environ.*, 112, 3833–3845, <https://doi.org/10.1016/j.rse.2008.06.006>, 2008.
- Jobbagy, E. G. and Jackson, R. B.: The Vertical Distribution of Soil Organic Carbon and Its Relation to Climate and Vegetation, *Ecol. Appl.*, 10, 423–436, <https://doi.org/10.2307/2641104>, 2000.
- Joiner, J., Yoshida, Y., Zhang, Y., Duveiller, G., Jung, M., Lyapustin, A., Wang, Y., and Tucker, C. J.: Estimation of Terrestrial Global Gross Primary Production (GPP) with Satellite Data-Driven Models and Eddy Covariance Flux Data, *Remote Sens.*, 10, 1346, <https://doi.org/10.3390/rs10091346>, 2018.
- Jordan, C. F.: Derivation of Leaf-Area Index from Quality of Light on the Forest Floor, *Ecology*, 50, 663–666, <https://doi.org/10.2307/1936256>, 1969.
- Jung, M., Reichstein, M., Margolis, H. A., Cescatti, A., Richardson, A. D., Arain, M. A., Arneth, A., Bernhofer, C., Bonal, D., Chen, J., Gianelle, D., Gobron, N., Kiely, G., Kutsch, W., Lasslop, G., Law, B. E., Lindroth, A., Merbold, L., Montagnani, L., Moors, E. J., Papale, D., Sottocornola, M., Vaccari, F., and Williams, C.: Global patterns of land-atmosphere fluxes of carbon dioxide, latent heat, and sensible heat derived from eddy covariance, satellite, and meteorological observations, *J. Geophys. Res.-Biogeo.*, 116, G00J07, <https://doi.org/10.1029/2010JG001566>, 2011.
- Jung, M., Koirala, S., Weber, U., Ichii, K., Gans, F., Camps-Valls, G., Papale, D., Schwalm, C., Tramontana, G., and Reichstein, M.: The FLUXCOM ensemble of global land-atmosphere energy fluxes, *Sci. Data*, 6, 74, <https://doi.org/10.1038/s41597-019-0076-8>, 2019.
- Juszczak, R., Uzdzička, B., Stróżecki, M., and Sakowska, K.: Improving remote estimation of winter crops gross ecosystem production by inclusion of leaf area index in a spectral model, *PeerJ*, 6, e5613, <https://doi.org/10.7717/peerj.5613>, 2018.
- Kong, J., Ryu, Y., Liu, J., Dechant, B., Rey-Sanchez, C., Shortt, R., Szutu, D., Verfaillie, J., Houborg, R., and Baldocchi, D. D.: Matching high resolution satellite data and flux tower footprints improves their agreement in photosynthesis estimates, *Agr. Forest Meteorol.*, 316, 108878, <https://doi.org/10.1016/j.agrformet.2022.108878>, 2022.
- Kormann, R. and Meixner, F. X.: An Analytical Footprint Model For Non-Neutral Stratification, *Bound.-Lay. Meteorol.*, 99, 207–224, <https://doi.org/10.1023/A:1018991015119>, 2001.
- Korres, W., Reichenau, T. G., and Schneider, K.: Corrigendum to “Patterns and scaling properties of surface soil moisture in an agricultural landscape: An ecohydrological modeling study” [*J. Hydrol.* 498 (2013) 89–102], *J. Hydrol.*, 519, 3691, <https://doi.org/10.1016/j.jhydrol.2014.09.006>, 2014.
- Lal, R., Smith, P., Jungkunst, H. F., Mitsch, W. J., Lehmann, J., Nair, P. K. R., McBratney, A. B., de Moraes Sá, J. C., Schneider, J., Zinn, Y. L., Skorupa, A. L. A., Zhang, H.-L., Minasny, B., Srinivasrao, C., and Ravindranath, N. H.: The carbon sequestration potential of terrestrial ecosystems, *J. Soil Water Conserv.*, 73, 145A–152A, <https://doi.org/10.2489/jswc.73.6.145A>, 2018.
- Lasslop, G., Reichstein, M., Papale, D., Richardson, A. D., Arneth, A., Barr, A., Stoy, P., and Wohlfahrt, G.: Separation of net ecosystem exchange into assimilation and respiration using a light response curve approach: critical issues and global evaluation, *Glob. Change Biol.*, 16, 187–208, <https://doi.org/10.1111/j.1365-2486.2009.02041.x>, 2010.
- Li, J., Yu, Q., Sun, X., Tong, X., Ren, C., Wang, J., Liu, E., Zhu, Z., and Yu, G.: Carbon dioxide exchange and the mechanism of environmental control in a farmland ecosystem in North China Plain, *Sci. China Ser. D*, 49, 226–240, <https://doi.org/10.1007/s11430-006-8226-1>, 2006.
- Lilienthal, H.: Optische Sensoren in der Landwirtschaft: Grundlagen und Konzepte, *Journal für Kulturpflanzen*, 66, 34–41, <https://doi.org/10.5073/JFK.2014.02.01> 2014.
- Lin, S., Li, J., Liu, Q., Li, L., Zhao, J., and Yu, W.: Evaluating the Effectiveness of Using Vegetation Indices Based on Red-Edge Reflectance from Sentinel-2 to Estimate Gross Primary Productivity, *Remote Sens.*, 11, 1303, <https://doi.org/10.3390/rs11111303>, 2019.
- Liu, F., Wang, C., and Wang, X.: Can vegetation index track the interannual variation in gross primary production of temperate deciduous forests?, *Ecological Processes*, 10, 51, <https://doi.org/10.1186/s13717-021-00324-2>, 2021.
- Liu, H. Q. and Huete, A. R.: A feedback based modification of the NDVI to minimize canopy background and atmospheric noise, *IEEE T. Geosci. Remote*, 33, 457–465, <https://doi.org/10.1109/TGRS.1995.8746027>, 1995.
- Lu, Y., Williams, I. N., Bagley, J. E., Torn, M. S., and Kuipers, L. M.: Representing winter wheat in the Community Land Model (version 4.5), *Geosci. Model Dev.*, 10, 1873–1888, <https://doi.org/10.5194/gmd-10-1873-2017>, 2017.
- Luyssaert, S., Jammot, M., Stoy, P. C., Estel, S., Pongratz, J., Ceschia, E., Churkina, G., Don, A., Erb, K., Ferlicoq, M., Gielen, B., Grünwald, T., Houghton, R. A., Klumpp, K., Knohl, A., Kolb, T., Kuemmerle, T., Laurila, T., Lohila, A., Loustau, D., McGrath, M. J., Meyfroidt, P., Moors, E. J., Naudts, K., Novick, K., Otto, J., Pilegaard, K., Pio, C. A., Rambal, S., Rebmann, C., Ryder, J., Suyker, A. E., Varlagin, A., Wattenbach, M., and Dolman, A. J.: Land management and land-cover change have impacts of similar magnitude on surface temperature, *Nat. Clim. Change*, 4, 389–393, <https://doi.org/10.1038/nclimate2196>, 2014.
- Ma, S., Baldocchi, D., Wolf, S., and Verfaillie, J.: Slow ecosystem responses conditionally regulate annual carbon balance over 15 years in Californian oak-grass savanna, *Agr. Forest Meteorol.*, 228–229, 252–264, <https://doi.org/10.1016/j.agrformet.2016.07.016>, 2016.
- Madugundu, R., Al-Gaadi, K. A., Tola, E., Kayad, A. G., and Jha, C. S.: Estimation of gross primary production of irrigated maize using Landsat-8 imagery and Eddy Covariance data, *Saudi J. Biol. Sci.*, 24, 410–420, <https://doi.org/10.1016/j.sjbs.2016.10.003>, 2017.
- Mahadevan, P., Wofsy, S. C., Matross, D. M., Xiao, X., Dunn, A. L., Lin, J. C., Gerbig, C., Munger, J. W., Chow, V. Y., and Gottlieb, E. W.: A satellite-based biosphere parameterization for net ecosystem CO<sub>2</sub> exchange: Vegetation Photosynthesis and Respiration Model (VPRM), *Global Biogeochem. Cy.*, 22, GB2005, <https://doi.org/10.1029/2006GB002735>, 2008.
- Masialeli, I., Egbert, S., and Wardlow, B. D.: A Comparative Analysis of Phenological Curves for Major Crops in Kansas, *GIScience Remote Sens.*, 47, 241–259, <https://doi.org/10.2747/1548-1603.47.2.241>, 2010.
- Mauder, M. and Foken, T.: Documentation and instruction manual of the eddy covariance software package TK2, *Arbeitsergebnisse, Univ Bayreuth, Abt Mikrometeorol*, 26, p. 42, 2004.
- McFeeters, S. K.: The use of the Normalized Difference Water Index (NDWI) in the delineation of open

- water features, *Int. J. Remote Sens.*, 17, 1425–1432, <https://doi.org/10.1080/01431169608948714>, 1996.
- Medlyn, B. E.: Physiological basis of the light use efficiency model, *Tree Physiol.*, 18, 167–176, <https://doi.org/10.1093/treephys/18.3.167>, 1998.
- Minasny, B., Malone, B. P., McBratney, A. B., Angers, D. A., Arrouays, D., Chambers, A., Chaplot, V., Chen, Z.-S., Cheng, K., Das, B. S., Field, D. J., Gimona, A., Hedley, C. B., Hong, S. Y., Mandal, B., Marchant, B. P., Martin, M., McConkey, B. G., Mulder, V. L., O'Rourke, S., Richer-de-Forges, A. C., Odeh, I., Padarian, J., Paustian, K., Pan, G., Poggio, L., Savin, I., Stolbovov, V., Stockmann, U., Sulae-man, Y., Tsui, C.-C., Vågen, T.-G., van Wesemael, B., and Winowiecki, L.: Soil carbon 4 per mille, *Geoderma*, 292, 59–86, <https://doi.org/10.1016/j.geoderma.2017.01.002>, 2017.
- Moureaux, C., Debaq, A., Hoyaux, J., Suleau, M., Tourneur, D., Vancutsem, F., Bodson, B., and Aubinet, M.: Carbon balance assessment of a Belgian winter wheat crop (*Triticum aestivum* L.), *Glob. Change Biol.*, 14, 1353–1366, <https://doi.org/10.1111/j.1365-2486.2008.01560.x>, 2008.
- Myneni, R. B. and Williams, D. L.: On the relationship between FAPAR and NDVI, *Remote Sens. Environ.*, 49, 200–211, [https://doi.org/10.1016/0034-4257\(94\)90016-7](https://doi.org/10.1016/0034-4257(94)90016-7), 1994.
- Nash, J. E. and Sutcliffe, J. V.: River flow forecasting through conceptual models part I – A discussion of principles, *J. Hydrol.*, 10, 282–290, [https://doi.org/10.1016/0022-1694\(70\)90255-6](https://doi.org/10.1016/0022-1694(70)90255-6), 1970.
- Noumonvi, K. D., Ferlan, M., Eler, K., Alberti, G., Peressotti, A., and Cerasoli, S.: Estimation of Carbon Fluxes from Eddy Covariance Data and Satellite-Derived Vegetation Indices in a Karst Grassland (Podgorski Kras, Slovenia), *Remote Sens.*, 11, 649, <https://doi.org/10.3390/rs11060649>, 2019.
- Olofsson, P., Lagergren, F., Lindroth, A., Lindström, J., Klemmedtsson, L., Kutsch, W., and Eklundh, L.: Towards operational remote sensing of forest carbon balance across Northern Europe, *Biogeosciences*, 5, 817–832, <https://doi.org/10.5194/bg-5-817-2008>, 2008.
- Pabon-Moreno, D. E., Migliavacca, M., Reichstein, M., and Mahecha, M. D.: On the Potential of Sentinel-2 for Estimating Gross Primary Production, *IEEE T. Geosci. Remote.*, 60, 1–12, <https://doi.org/10.1109/TGRS.2022.3152272>, 2022.
- Papale, D., Reichstein, M., Aubinet, M., Canfora, E., Bernhofer, C., Kutsch, W., Longdoz, B., Rambal, S., Valentini, R., Vesala, T., and Yakir, D.: Towards a standardized processing of Net Ecosystem Exchange measured with eddy covariance technique: algorithms and uncertainty estimation, *Biogeosciences*, 3, 571–583, <https://doi.org/10.5194/bg-3-571-2006>, 2006.
- Pastorello, G., Trotta, C., Canfora, E., Chu, H., Christianson, D., Cheah, Y.-W., Poindexter, C., Chen, J., Elbashandy, A., Humphrey, M., Isaac, P., Polidori, D., Reichstein, M., Ribeca, A., van Ingen, C., Vuichard, N., Zhang, L., Amiro, B., Ammann, C., Arain, M. A., Ardö, J., Arkebauer, T., Arndt, S. K., Arriga, N., Aubinet, M., Aurela, M., Baldocchi, D., Barr, A., Beamesderfer, E., Marchesini, L. B., Bergeron, O., Beringer, J., Bernhofer, C., Berveiller, D., Billesbach, D., Black, T. A., Blanken, P. D., Bohrer, G., Boike, J., Bolstad, P. V., Bonal, D., Bonnefond, J.-M., Bowling, D. R., Bracho, R., Brodeur, J., Brümmer, C., Buchmann, N., Burban, B., Burns, S. P., Buysse, P., Cale, P., Cavagna, M., Cellier, P., Chen, S., Chini, I., Christensen, T. R., Cleverly, J., Collalti, A., Consalvo, C., Cook, B. D., Cook, D., Coursolle, C., Cremonese, E., Curtis, P. S., D'Andrea, E., da Rocha, H., Dai, X., Davis, K. J., Cinti, B. D., Grandcourt, A. d., Ligne, A. D., De Oliveira, R. C., Delpierre, N., Desai, A. R., Di Bella, C. M., Tommasi, P. d., Dolman, H., Domingo, F., Dong, G., Dore, S., Duce, P., Dufrêne, E., Dunn, A., Dušek, J., Eamus, D., Eichelmann, U., ElKhidir, H. A. M., Eugster, W., Ewenz, C. M., Ewers, B., Famulari, D., Fares, S., Feigenwinter, I., Feitz, A., Fensholt, R., Filippa, G., Fischer, M., Frank, J., Galvagno, M., Gharun, M., Gianelle, D., Gielen, B., Gioli, B., Gitelson, A., Goded, I., Goeckede, M., Goldstein, A. H., Gough, C. M., Goulden, M. L., Graf, A., Griebel, A., Gruening, C., Grünwald, T., Hammerle, A., Han, S., Han, X., Hansen, B. U., Hanson, C., Hatakka, J., He, Y., Hehn, M., Heinesch, B., Hinko-Najera, N., Hörtnagl, L., Hutley, L., Ibrom, A., Ikawa, H., Jackowicz-Korczynski, M., Janouš, D., Jans, W., Jassal, R., Jiang, S., Kato, T., Khomik, M., Klatt, J., Knohl, A., Knox, S., Kobayashi, H., Koerber, G., Kolle, O., Kosugi, Y., Kotani, A., Kowalski, A., Kruijt, B., Kurbatova, J., Kutsch, W. L., Kwon, H., Launiainen, S., Laurila, T., Law, B., Leuning, R., Li, Y., Liddell, M., Limousin, J.-M., Lion, M., Liska, A. J., Lohila, A., López-Ballesteros, A., López-Blanco, E., Loubet, B., Loustau, D., Lucas-Moffat, A., Lüers, J., Ma, S., Macfarlane, C., Magliulo, V., Maier, R., Mammarella, I., Manca, G., Marcolla, B., Margolis, H. A., Marras, S., Massman, W., Mastepanov, M., Matamala, R., Matthes, J. H., Mazzenga, F., McCaughey, H., McHugh, I., McMillan, A. M. S., Merbold, L., Meyer, W., Meyers, T., Miller, S. D., Minerbi, S., Moderow, U., Monson, R. K., Montagnani, L., Moore, C. E., Moors, E., Moreaux, V., Moureaux, C., Munger, J. W., Nakai, T., Neiryneck, J., Nesic, Z., Nicolini, G., Noormets, A., Northwood, M., Nosoetto, M., Nouvellon, Y., Novick, K., Oechel, W., Olesen, J. E., Ourcival, J.-M., Papuga, S. A., Parmentier, F.-J., Paul-Limoges, E., Pavelka, M., Peichl, M., Pendall, E., Phillips, R. P., Pilegaard, K., Pirk, N., Posse, G., Powell, T., Prasse, H., Prober, S. M., Rambal, S., Rannik, Ü., Raz-Yaseef, N., Rebmann, C., Reed, D., Dios, V. R. d., Restrepo-Coupe, N., Reverter, B. R., Roland, M., Sabbatini, S., Sachs, T., Saleska, S. R., Sánchez-Cañete, E. P., Sanchez-Mejia, Z. M., Schmid, H. P., Schmidt, M., Schneider, K., Schrader, F., Schroder, I., Scott, R. L., Sedláč, P., Serrano-Ortiz, P., Shao, C., Shi, P., Shironya, I., Siebicke, L., Šigut, L., Silberstein, R., Sirca, C., Spano, D., Steinbrecher, R., Stevens, R. M., Sturtevant, C., Suyker, A., Tagesson, T., Takahashi, S., Tang, Y., Tapper, N., Thom, J., Tomassucci, M., Tuovinen, J.-P., Urbanski, S., Valentini, R., van der Molen, M., van Gorsel, E., van Huissteden, K., Varlagin, A., Verfaillie, J., Vesala, T., Vincke, C., Vitale, D., Vygodskaya, N., Walker, J. P., Walter-Shea, E., Wang, H., Weber, R., Westermann, S., Wille, C., Wofsy, S., Wohlfahrt, G., Wolf, S., Woodgate, W., Li, Y., Zampedri, R., Zhang, J., Zhou, G., Zona, D., Agarwal, D., Biraud, S., Torn, M., and Papale, D.: The FLUXNET2015 dataset and the ONEFlux processing pipeline for eddy covariance data, *Sci. Data*, 7, 225, <https://doi.org/10.1038/s41597-020-0534-3>, 2020.
- Peng, Y. and Gitelson, A. A.: Remote estimation of gross primary productivity in soybean and maize based on total crop chlorophyll content, *Remote Sens. Environ.*, 117, 440–448, <https://doi.org/10.1016/j.rse.2011.10.021>, 2012.
- Pique, G., Fieuzal, R., Al Bitar, A., Veloso, A., Tallec, T., Brut, A., Ferlicoq, M., Zawilski, B., Dejoux, J.-F., Gibrin, H., and Ceschia, E.: Estimation of daily CO<sub>2</sub> fluxes and of the components of the carbon budget for winter wheat by the assimilation of Sentinel

- 2-like remote sensing data into a crop model, *Geoderma*, 376, 114428, <https://doi.org/10.1016/j.geoderma.2020.114428>, 2020.
- Qi, J., Marsett, R., Heilman, P., Bieden-bender, S., Moran, S., Goodrich, D., and Weltz, M.: RANGES improves satellite-based information and land cover assessments in southwest United States, *Eos, Transactions American Geophysical Union*, 83, 601–606, <https://doi.org/10.1029/2002EO000411>, 2002.
- R Core Team: R: A language and environment for statistical computing, R Foundation for Statistical Computing, Vienna, Austria, <https://www.R-project.org/> (last access: 13 August 2024), 2021.
- Rahman, A. F., Sims, D. A., Cordova, V. D., and El-Masri, B. Z.: Potential of MODIS EVI and surface temperature for directly estimating per-pixel ecosystem C fluxes, *Geophys. Res. Lett.*, 32, L19404, <https://doi.org/10.1029/2005GL024127>, 2005.
- Rawson, H., Gardner, P., and Long, M.: Sources of Variation in Specific Leaf Area in Wheat Grown at High Temperature, *Funct. Plant Biol.*, 14, 287–298, <https://doi.org/10.1071/PP9870287>, 1987.
- Reichstein, M., Falge, E., Baldocchi, D., Papale, D., Aubinet, M., Berbigier, P., Bernhofer, C., Buchmann, N., Gilmanov, T., Granier, A., Grünwald, T., Havráňková, K., Ilvesniemi, H., Janous, D., Knohl, A., Laurila, T., Lohila, A., Loustau, D., Matteucci, G., Meyers, T., Miglietta, F., Ourcival, J.-M., Pumpanen, J., Rambal, S., Rotenberg, E., Sanz, M., Tenhunen, J., Seufert, G., Vaccari, F., Vesala, T., Yakir, D., and Valentini, R.: On the separation of net ecosystem exchange into assimilation and ecosystem respiration: review and improved algorithm, *Glob. Change Biol.*, 11, 1424–1439, <https://doi.org/10.1111/j.1365-2486.2005.001002.x>, 2005.
- Rouse, J. W., Haas, R. H., Schell, J. A., and Deering, D. W.: Monitoring vegetation systems in the great plains with ERTS, Third ERTS Symposium, NASA SP-351 I, 309–317, 1974.
- Rumpel, C., Amiraslani, F., Chenu, C., Garcia Cardenas, M., Kaonga, M., Koutika, L.-S., Ladha, J., Madari, B., Shirato, Y., Smith, P., Soudi, B., Soussana, J.-F., Whitehead, D., and Wollenberg, E.: The 4p1000 initiative: Opportunities, limitations and challenges for implementing soil organic carbon sequestration as a sustainable development strategy, *Ambio*, 49, 350–360, <https://doi.org/10.1007/s13280-019-01165-2>, 2020.
- Running, S. W., Nemani, R. R., Heinsch, F. A., Zhao, M., Reeves, M., and Hashimoto, H.: A Continuous Satellite-Derived Measure of Global Terrestrial Primary Production, *BioScience*, 54, 547–560, [https://doi.org/10.1641/0006-3568\(2004\)054\[0547:Acsmog\]2.0.Co;2](https://doi.org/10.1641/0006-3568(2004)054[0547:Acsmog]2.0.Co;2), 2004.
- Sanderman, J., Hengl, T., and Fiske, G. J.: Soil carbon debt of 12,000 years of human land use, *P. Natl. Acad. Sci. USA*, 114, 9575–9580, <https://doi.org/10.1073/pnas.1706103114>, 2017.
- Schmidt, M., Reichenau, T. G., Fiener, P., and Schneider, K.: The carbon budget of a winter wheat field: An eddy covariance analysis of seasonal and inter-annual variability, *Agr. Forest Meteorol.*, 165, 114–126, <https://doi.org/10.1016/j.agrformet.2012.05.012>, 2012.
- Siemens, J., Pacholski, A., Heiduk, K., Giesemann, A., Schulte, U., Dechow, R., Kaupenjohann, M., and Weigel, H.-J.: Elevated air carbon dioxide concentrations increase dissolved carbon leaching from a cropland soil, *Biogeochemistry*, 108, 135–148, <https://doi.org/10.1007/s10533-011-9584-0>, 2012.
- Sims, D. A., Rahman, A. F., Cordova, V. D., El-Masri, B. Z., Baldocchi, D. D., Flanagan, L. B., Goldstein, A. H., Hollinger, D. Y., Misson, L., Monson, R. K., Oechel, W. C., Schmid, H. P., Wofsy, S. C., and Xu, L.: On the use of MODIS EVI to assess gross primary productivity of North American ecosystems, *J. Geophys. Res.-Biogeo.*, 111, G04015, <https://doi.org/10.1029/2006JG000162>, 2006.
- Smith, P., Lanigan, G., Kutsch, W. L., Buchmann, N., Eugster, W., Aubinet, M., Ceschia, E., Béziat, P., Yeluripati, J. B., Osborne, B., Moors, E. J., Brut, A., Wattenbach, M., Saunders, M., and Jones, M.: Measurements necessary for assessing the net ecosystem carbon budget of croplands, *Agr. Ecosyst. Environ.*, 139, 302–315, <https://doi.org/10.1016/j.agee.2010.04.004>, 2010.
- Spinosa, A., Fuentes-Monjaraz, M. A., and El Serafy, G.: Assessing the Use of Sentinel-2 Data for Spatio-Temporal Upscaling of Flux Tower Gross Primary Productivity Measurements, *Remote Sens.*, 15, 562, <https://doi.org/10.3390/rs15030562>, 2023.
- Suleau, M., Moureaux, C., Dufrenoy, D., Buysse, P., Bodson, B., Destain, J.-P., Heinesch, B., Debacq, A., and Aubinet, M.: Respiration of three Belgian crops: Partitioning of total ecosystem respiration in its heterotrophic, above- and below-ground autotrophic components, *Agr. Forest Meteorol.*, 151, 633–643, <https://doi.org/10.1016/j.agrformet.2011.01.012>, 2011.
- Sus, O., Williams, M., Bernhofer, C., Béziat, P., Buchmann, N., Ceschia, E., Doherty, R., Eugster, W., Grünwald, T., Kutsch, W., Smith, P., and Wattenbach, M.: A linked carbon cycle and crop developmental model: Description and evaluation against measurements of carbon fluxes and carbon stocks at several European agricultural sites, *Agr. Ecosyst. Environ.*, 139, 402–418, <https://doi.org/10.1016/j.agee.2010.06.012>, 2010.
- Tramontana, G., Ichii, K., Camps-Valls, G., Tomelleri, E., and Papale, D.: Uncertainty analysis of gross primary production upscaling using Random Forests, remote sensing and eddy covariance data, *Remote Sens. Environ.*, 168, 360–373, <https://doi.org/10.1016/j.rse.2015.07.015>, 2015.
- Tramontana, G., Jung, M., Schwalm, C. R., Ichii, K., Camps-Valls, G., Ráduly, B., Reichstein, M., Arain, M. A., Cescatti, A., Kiely, G., Merbold, L., Serrano-Ortiz, P., Sickert, S., Wolf, S., and Papale, D.: Predicting carbon dioxide and energy fluxes across global FLUXNET sites with regression algorithms, *Biogeosciences*, 13, 4291–4313, <https://doi.org/10.5194/bg-13-4291-2016>, 2016.
- Van Oosterom, E. J. and Acevedo, E.: Leaf area and crop growth in relation to phenology of barley in Mediterranean environments, *Plant Soil*, 148, 223–237, 1993.
- Vuichard, N., Ciais, P., Viovy, N., Li, L., Ceschia, E., Wattenbach, M., Bernhofer, C., Emmel, C., Grünwald, T., Jans, W., Loubet, B., and Wu, X.: Simulating the net ecosystem CO<sub>2</sub> exchange and its components over winter wheat cultivation sites across a large climate gradient in Europe using the ORCHIDEE-STICS generic model, *Agr. Ecosyst. Environ.*, 226, 1–17, <https://doi.org/10.1016/j.agee.2016.04.017>, 2016.
- Waldo, S., Chi, J., Pressley, S. N., O’Keeffe, P., Pan, W. L., Brooks, E. S., Huggins, D. R., Stöckle, C. O., and Lamb, B. K.: Assessing carbon dynamics at high and low rainfall agricultural sites in the inland Pacific Northwest US using the eddy covariance method, *Agr. Forest Meteorol.*, 218–219, 25–36, <https://doi.org/10.1016/j.agrformet.2015.11.018>, 2016.
- Wang, Q., Tenhunen, J., Dinh, N. Q., Reichstein, M., Vesala, T., and Keronen, P.: Similarities in ground- and satellite-based NDVI time series and their relationship to physiological activity of a

- Scots pine forest in Finland, *Remote Sens. Environ.*, 93, 225–237, <https://doi.org/10.1016/j.rse.2004.07.006>, 2004.
- Wang, Y., Hu, C., Dong, W., Li, X., Zhang, Y., Qin, S., and Oenema, O.: Carbon budget of a winter-wheat and summer-maize rotation cropland in the North China Plain, *Agr. Ecosyst. Environ.*, 206, 33–45, <https://doi.org/10.1016/j.agee.2015.03.016>, 2015.
- Wattenbach, M., Gottschalk, P., Hattermann, F., Rachimow, C., Flechsig, M., and Smith, P.: A framework for assessing uncertainty in ecosystem models, iEMSs Third Biennial Meeting: “Summit on Environmental Modelling and Software”, Burlington, USA, 2006.
- Wattenbach, M., Sus, O., Vuichard, N., Lehuger, S., Gottschalk, P., Li, L., Leip, A., Williams, M., Tomelleri, E., Kutsch, W. L., Buchmann, N., Eugster, W., Dietiker, D., Aubinet, M., Ceschia, E., BÅ@ziat, P., Grünwald, T., Hastings, A., Osborne, B., Ciais, P., Cellier, P., and Smith, P.: The carbon balance of European croplands: A cross-site comparison of simulation models, *Agr. Ecosyst. Environ.*, 139, 419–453, <https://doi.org/10.1016/j.agee.2010.08.004>, 2010.
- Weaver, S. E., Kropff, M., and Cousens, R. D.: A simulation model of competition between winter wheat and *Avena fatua* for light, *Ann. Appl. Biol.*, 124, 315–331, <https://doi.org/10.1111/j.1744-7348.1994.tb04136.x>, 1994.
- Wohlfahrt, G., Pilloni, S., Hörtnagl, L., and Hammerle, A.: Estimating carbon dioxide fluxes from temperate mountain grasslands using broad-band vegetation indices, *Biogeosciences*, 7, 683–694, <https://doi.org/10.5194/bg-7-683-2010>, 2010.
- Wolanin, A., Camps-Valls, G., Gómez-Chova, L., Mateo-García, G., van der Tol, C., Zhang, Y., and Guanter, L.: Estimating crop primary productivity with Sentinel-2 and Landsat 8 using machine learning methods trained with radiative transfer simulations, *Remote Sens. Environ.*, 225, 441–457, <https://doi.org/10.1016/j.rse.2019.03.002>, 2019.
- Wutzler, T., Lucas-Moffat, A., Migliavacca, M., Knauer, J., Sickel, K., Šigut, L., Menzer, O., and Reichstein, M.: Basic and extensible post-processing of eddy covariance flux data with REddyProc, *Biogeosciences*, 15, 5015–5030, <https://doi.org/10.5194/bg-15-5015-2018>, 2018.
- Xiao, J., Zhuang, Q., Baldocchi, D. D., Law, B. E., Richardson, A. D., Chen, J., Oren, R., Starr, G., Noormets, A., Ma, S., Verma, S. B., Wharton, S., Wofsy, S. C., Bolstad, P. V., Burns, S. P., Cook, D. R., Curtis, P. S., Drake, B. G., Falk, M., Fischer, M. L., Foster, D. R., Gu, L., Hadley, J. L., Hollinger, D. Y., Katul, G. G., Litvak, M., Martin, T. A., Matamala, R., McNulty, S., Meyers, T. P., Monson, R. K., Munger, J. W., Oechel, W. C., Paw U, K. T., Schmid, H. P., Scott, R. L., Sun, G., Suyker, A. E., and Torn, M. S.: Estimation of net ecosystem carbon exchange for the conterminous United States by combining MODIS and AmeriFlux data, *Agr. Forest Meteorol.*, 148, 1827–1847, <https://doi.org/10.1016/j.agrformet.2008.06.015>, 2008.
- Xiao, J., Zhuang, Q., Law, B. E., Chen, J., Baldocchi, D. D., Cook, D. R., Oren, R., Richardson, A. D., Wharton, S., Ma, S., Martin, T. A., Verma, S. B., Suyker, A. E., Scott, R. L., Monson, R. K., Litvak, M., Hollinger, D. Y., Sun, G., Davis, K. J., Bolstad, P. V., Burns, S. P., Curtis, P. S., Drake, B. G., Falk, M., Fischer, M. L., Foster, D. R., Gu, L., Hadley, J. L., Katul, G. G., Matamala, R., McNulty, S., Meyers, T. P., Munger, J. W., Noormets, A., Oechel, W. C., Paw U, K. T., Schmid, H. P., Starr, G., Torn, M. S., and Wofsy, S. C.: A continuous measure of gross primary production for the conterminous United States derived from MODIS and AmeriFlux data, *Remote Sens. Environ.*, 114, 576–591, <https://doi.org/10.1016/j.rse.2009.10.013>, 2010.
- Xiao, J., Zhuang, Q., Law, B. E., Baldocchi, D. D., Chen, J., Richardson, A. D., Melillo, J. M., Davis, K. J., Hollinger, D. Y., Wharton, S., Oren, R., Noormets, A., Fischer, M. L., Verma, S. B., Cook, D. R., Sun, G., McNulty, S., Wofsy, S. C., Bolstad, P. V., Burns, S. P., Curtis, P. S., Drake, B. G., Falk, M., Foster, D. R., Gu, L., Hadley, J. L., Katul, G. G., Litvak, M., Ma, S., Martin, T. A., Matamala, R., Meyers, T. P., Monson, R. K., Munger, J. W., Oechel, W. C., Paw, U. K. T., Schmid, H. P., Scott, R. L., Starr, G., Suyker, A. E., and Torn, M. S.: Assessing net ecosystem carbon exchange of U.S. terrestrial ecosystems by integrating eddy covariance flux measurements and satellite observations, *Agr. Forest Meteorol.*, 151, 60–69, <https://doi.org/10.1016/j.agrformet.2010.09.002>, 2011.
- Xu, H.: Modification of normalised difference water index (NDWI) to enhance open water features in remotely sensed imagery, *Int. J. Remote Sens.*, 27, 3025–3033, <https://doi.org/10.1080/01431160600589179>, 2006.
- Yuan, W., Cai, W., Xia, J., Chen, J., Liu, S., Dong, W., Merbold, L., Law, B., Arain, A., Beringer, J., Bernhofer, C., Black, A., Blanken, P. D., Cescatti, A., Chen, Y., Francois, L., Gianelle, D., Janssens, I. A., Jung, M., Kato, T., Kiely, G., Liu, D., Marcolla, B., Montagnani, L., Raschi, A., Rouspard, O., Varlagin, A., and Wohlfahrt, G.: Global comparison of light use efficiency models for simulating terrestrial vegetation gross primary production based on the LaThuile database, *Agr. Forest Meteorol.*, 192–193, 108–120, <https://doi.org/10.1016/j.agrformet.2014.03.007>, 2014.
- Zhang, Q., Lei, H.-M., and Yang, D.-W.: Seasonal variations in soil respiration, heterotrophic respiration and autotrophic respiration of a wheat and maize rotation cropland in the North China Plain, *Agr. Forest Meteorol.*, 180, 34–43, <https://doi.org/10.1016/j.agrformet.2013.04.028>, 2013.
- Zhou, Y., Zhang, L., Xiao, J., Chen, S., Kato, T., and Zhou, G.: A Comparison of Satellite-Derived Vegetation Indices for Approximating Gross Primary Productivity of Grasslands, *Rangeland Ecol. Manag.*, 67, 9–18, <https://doi.org/10.2111/REM-D-13-00059.1>, 2014.
- Zomer, R. J., Bossio, D. A., Sommer, R., and Verchot, L. V.: Global Sequestration Potential of Increased Organic Carbon in Cropland Soils, *Sci. Rep.*, 7, 15554, <https://doi.org/10.1038/s41598-017-15794-8>, 2017.